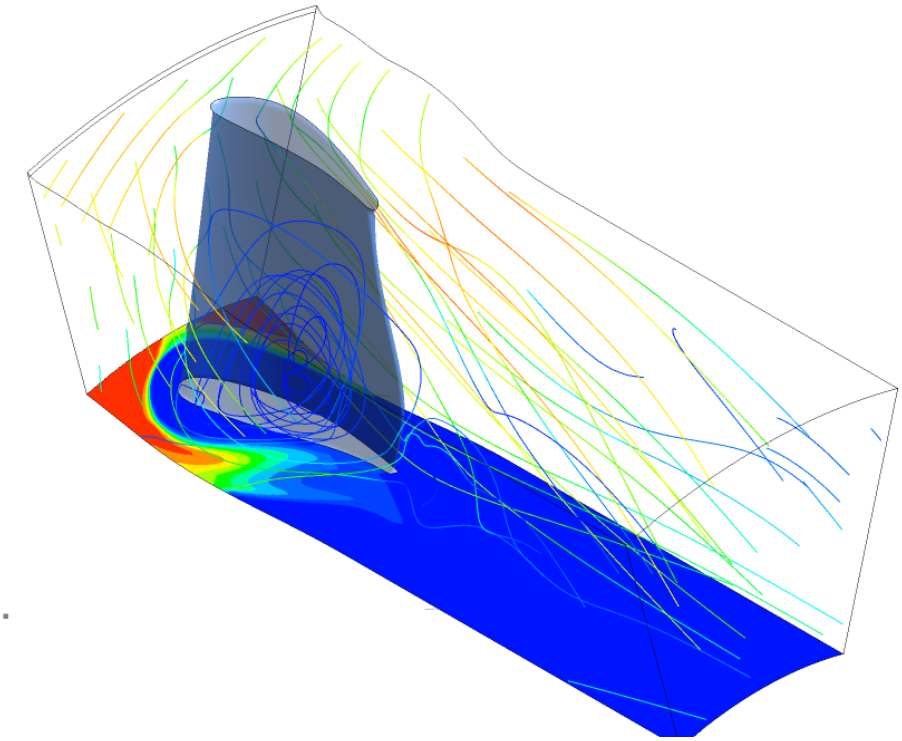

The Numerical Investigation of Outlet Guide Vane Heat Transfer

Master's thesis in Applied Mechanics

ARAVIND MURALI

DEPARTMENT OF MECHANICS AND MARITIME SCIENCE

CHALMERS UNIVERSITY OF TECHNOLOGY
Gothenburg, Sweden 2023
www.chalmers.se

Master's thesis 2023

The Numerical Investigation of Outlet Guide Vane Heat Transfer

ARAVIND MURALI

CHALMERS
UNIVERSITY OF TECHNOLOGY

Department of Mechanics and Maritime Sciences
Division of Fluid Mechanics
Chalmers University of Technology
Gothenburg, Sweden 2023

The Numerical Investigation of Outlet Guide Vane Heat Transfer
ARAVIND MURALI

Supervisor: Abrahamsson Hans, GKN Aerospace Sweden
Examiner: Valery Chernoray, Department of Mechanics and Maritime Sciences

Master's Thesis 2023
Department of Mechanics and Maritime Sciences
Division of Fluid Dynamics
Chalmers University of Technology
SE-412 96 Gothenburg
Telephone +46 31 772 1000

Cover: Film Coefficient Contour : Cold film breakup - off design analysis.

Typeset in LaTeX
Printed by Chalmers Reproservice
Gothenburg, Sweden 2023

The Numerical Investigation of Outlet Guide Vane Heat Transfer
ARAVIND MURALI
Department of Mechanics and Maritime Sciences
Chalmers University of Technology

Abstract

Aero-engine components are subjected to high thermal loads and uneven temperature distribution during working conditions. The heat transfer investigation plays a significant role in the development and analysis of these structures. To increase the understanding of the heat transfer over a Turbine Rear Structure(TRS), tests are conducted at experimental facilities giving good insights and valuable inputs for possible design improvements.

The primary objective of this thesis is to utilize the available heat transfer experimental data from the Chalmers LPT-OGV(Low Pressure Turbine-Outer Guide Vane) test rig to validate the CFD methodology for aero-thermal heat transfer analysis.

In this work, the CFD heat transfer predictions are compared to the heat transfer test data obtained from the LPT-OGV test rig which is capable of replicating realistic engine conditions. The same operating conditions as in the test facility are used on the CFD model to reproduce numerical results. A comparative analysis of heat transfer coefficients (HTC) is conducted between the CFD predictions and the experimental data obtained from the LPT-OGV test rig, considering both on-design and off-design cases. The wake shedding effects on heat transfer for off-design conditions is investigated using a transient solver. Furthermore, a detailed analysis is conducted to examine the formation of film coefficient profiles over the hub region, which are then compared against the corresponding experimental data

The findings revealed that, in general, transition of flow is observed over the suction side of OGV. CFD simulations tend to under predict the experimental HTC values. The SST transition model captures the transition effect, but predicts an earlier transition when compared with experimental data. The film coefficient profiles formed through CFD exhibited similarity to experimental profiles, although the experimental values displayed greater dispersion. These results contribute to the understanding and validation of CFD methodologies using experimental data, while also highlighting areas where further improvements are necessary

Keywords: CFD, Transition, Heat transfer, Turbine rear structure (TRS), Heat transfer coefficients (HTC).

Acknowledgements

First and foremost, I extend my heartfelt gratitude to my thesis supervisor, Hans Abrahamsson, at GKN Aerospace Engine Systems Sweden, for his unwavering support and guidance throughout this journey. Without his invaluable mentorship, this thesis would not have been accomplished. Hans has been available to assist me at all times, and the knowledge and experience I gained during the six months of working with him are truly immeasurable. His role as both a supervisor and mentor has been instrumental in my growth.

I would also like to express my sincere appreciation to Srikanth Deshpande, my CFD mentor, who has been incredibly supportive and available even during his vacation times. Without his guidance, completing this thesis would not have been possible. His support played a pivotal role in helping me navigate through the hurdles and advance in my thesis work.

Chalmers University has provided excellent support, and I am particularly grateful to Prof. Valery Chernoray from the Fluid Mechanics Department for taking the time to be the examiner for this project. Additionally, I would like to thank Valentin Vikhorev for his immense support in providing test rig data and valuable insights. The time he dedicated to deep discussions and analysis of the work was truly invaluable.

My heartfelt thanks go out to my friends and family for their immense support and encouragement throughout this journey. And lastly, I would like to acknowledge myself for believing in my abilities and staying strong through all the challenges faced.

Aravind Murali, Gothenburg, July 2023

List of Acronyms

Below is the list of acronyms that have been used throughout this thesis listed in alphabetical order:

CFD	Computational Fluid Dynamics
LPT	Low Pressure Turbine
OGV	Outer Guide Vane
TRS	Turbine Rare Structure
AOA	Angle Of Attack
HTC	Heat Transfer Coefficient
Nu	Nusselt Number
Pr	Prandtl Number
ϕ	Flow Coefficient
θ	Film Coefficient

Nomenclature

Below is the nomenclature of indices, sets, parameters, and variables that have been used throughout this thesis.

Variables

h	Heat Transfer Coefficient
T	Temperature
Q	Rate of Heat transfer
h	Heat Transfer Coefficient
q	Total Surface Heat Flux
Δ	Change in Temperature
A	Area of surface in contact
ρ	Density
u	Flow speed
L	Characteristic Length
μ	Dynamic Viscosity
ν	Kinematic Viscosity
α	Thermal Diffusivity
k	Thermal Conductivity
$\bar{v}_i$	Mean Velocity component
v'_i	Fluctuating Velocity component
$\bar{p}$	Mean Pressure component
p'	Fluctuating pressure component
k	Turbulent Kinetic Energy
ϵ	Turbulent Dissipation rate
ω	Specific Dissipation rate

Contents

List of Figures

List of Tables

1
Introduction

1.1 Background

Aero engines are powerful mechanical machines which are designed to produce enough thrust to propel aircraft through the air. At GKN Aerospace Trollhattan, various aero-engine components are designed and manufactured. One such component is the Turbine Rear Structure (TRS) which is located at the aft end of the engine. This component mounts the engine frame to the aircraft body providing structural support, providing passages for oil, cooling and guiding the exit hot-exhaust axially with the help of static outer guide vanes (OGV). Figure 1.1 shows a pictorial representation of TRS.

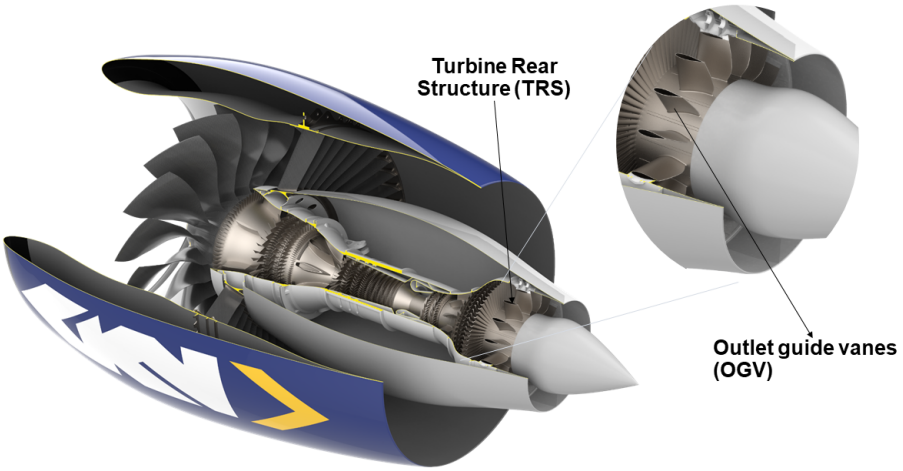

Figure 1.1: Aero-Engine with TRS

The TRS is subjected to high temperatures around approx 650°C during working conditions. This high temperature can induce thermal stresses/loads over TRS's surface, causing them to deform and crack eventually. Additionally, the TRS can also experience cyclic fatigue due to uneven temperature distribution which potentially leads to fatigue failure in the domain. To prevent potential issues, advanced cooling methods are employed to effectively manage heat transfer within the TRS domain. At GKN Aerospace Sweden, a comprehensive approach involving both experimental and computational heat transfer analyses is undertaken to gain a deeper understanding of the heat transfer characteristics over the TRS.

Modern aero-engines utilize bleed air from the compressor and direct it towards the turbine domain via a small passage. This cold bleed air is ejected through the cavity between the TRS hub and the rotor domain. This purge flow passage creates a thin cold film over the surface of the TRS hub. The formed cold film has a significant impact on the end wall heat transfer. A visual representation of cold film due to purge flow is shown in 1.2.

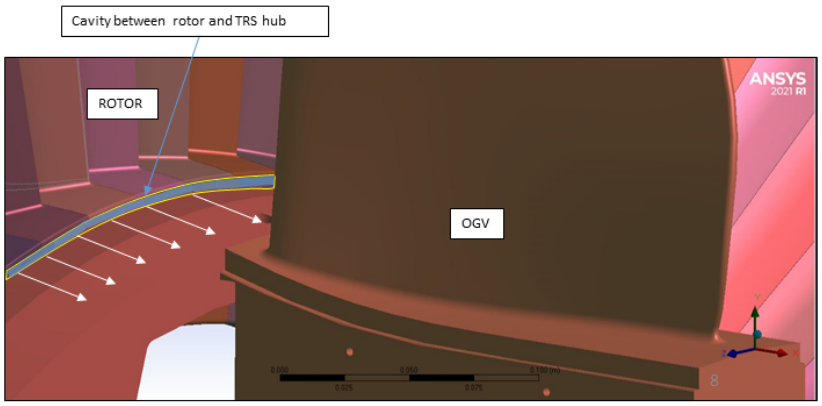

Figure 1.2: Purge Flow

1.2 Experimental Facility at Chalmers

Chalmers University has an experimental facility equipped with an LPT-OGV test rig setup which is utilized for various heat transfer and aerodynamic measurements.

This facility is a closed wind tunnel driven by a centrifugal fan. The flow is directed to a diffuser followed by a heat exchanger to a settling chamber. In the end, the flow is accelerated through a contraction before entering the LPT Segment. The LPT-OGV setup consists of 1 stage of LPT followed by a TRS. The LPT is used to replicate the realistic engine boundary conditions to the inlet of the OGV domain. An illustration of the experimental facility is shown below for reference 1.3.

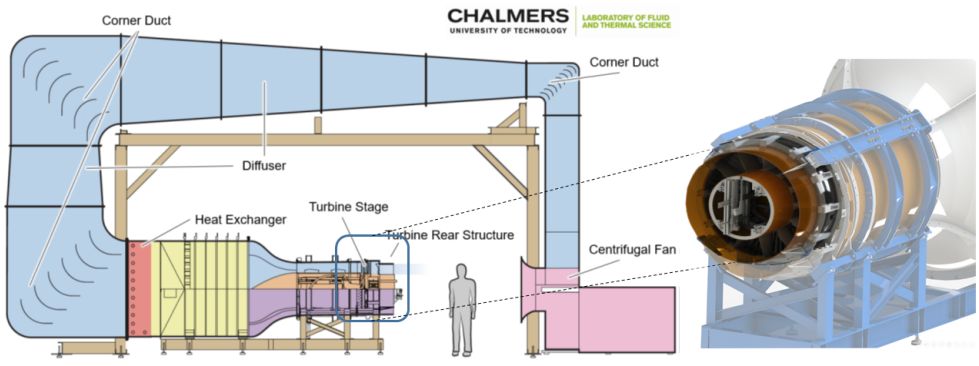

Figure 1.3: An Illustration of Experimental Facility[1]

The test facility utilizes infrared thermography for temperature measurement over the surface of OGV. A custom design vane is fitted to the TRS section which has an additional internal water flow passage as shown in the figure 1.4. Water at high temperatures is supplied through this passage to heat the surface of the TRS Vane. When the colder main flow passes through the TRS domain, the infrared camera captures the temperature over the surface of the OGV and end walls to measure the HTC.

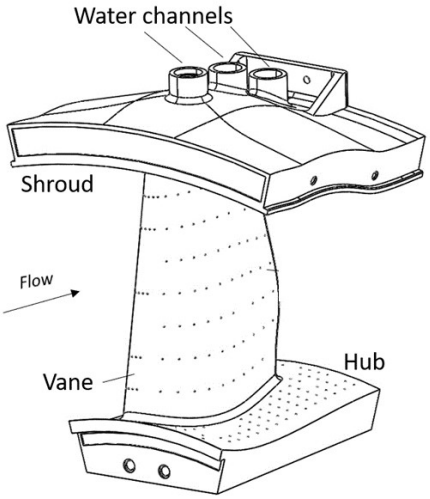

Figure 1.4: Vane with internal water passage

The LPT-OGV rig setup has an additional facility to replicate the hub purge flow. Figure 1.5 shows the illustration of this setup. A secondary flow is directed to the cavity between the rotor segment and the static OGV domain before the TRS. The flow travels through a circular pipe followed by a diffuser and exits through the cavity between the rotor domain and TRS. For ease of experimental measurements, the purge flow is intentionally heated to a higher temperature than the main incoming flow allowing to the evaluation of HTC and film coefficient.

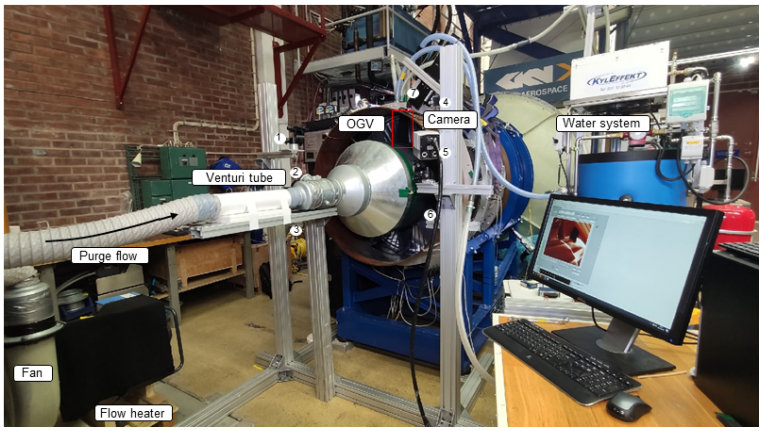

Figure 1.5: Purge flow experimental setup

1.3 Literature Review

The Chalmers LPT-OGV test rig facility has been continuously used for various aerodynamics and thermodynamic experimental measurements. The paper referenced in [1] presents a new approach for conducting heat transfer measurements using infrared thermography on the Chalmers LPT-OGV test rig. The findings from this study show the occurrence of a flow transition on the suction side of the OGV. In the present thesis work, the experimental heat transfer data obtained through infrared thermography from Chalmers LPT-OGV test rig is utilized for method validation of CFD. The research work done in [2] investigates the effect of HTC due to changes in incidence angle. The results show a remarkable increase in end wall HTC for the off-design case when compared with the on-design case. In [3], a detailed experiment heat transfer analysis is carried out in a linear cascade facility to investigate the end wall HTC. This investigation also revealed an increase in HTC for off-design analysis.

The research paper by Wang et al. (2016) [4] extensively examines the performance of various turbulence models in predicting HTC. Three different turbulence models, including the SST transition model, are utilized to evaluate the HTC over the vane. The study reveals that the k-ω model exhibits limitations in accurately predicting heat transfer, while the SST transition model offers improved predictions. In the research paper [5], the researchers conducted an experimental investigation to examine how reynolds number and incidence angle impact heat transfer. They observed that as the Reynolds number increases, there is a corresponding increase in heat transfer. Additionally, altering the incidence angle results in a shift in the transition point, which consequently leads to a significant change in the HTC.

The research paper referenced in [6] examines the impact of surface roughness on heat transfer in TRS by employing a 3D CFD model. This CFD model resembles the experimental setup for TRS in the LPT-OGV test rig at Chalmers. The present study employs this computational model to conduct further analysis and simulations. In [7], the work focuses on investigating the aerodynamic characteristics of the LPT-OGV test rig. A 1.5-stage 3D CFD model was employed, encompassing one stage of LPT followed by a stage of TRS. This 1.5-stage CFD model serves as the basis for the present work, which focuses on heat transfer simulation and analysis.

1.4 Aim

The primary objective of this thesis is to utilize the available heat transfer experimental data from the Chalmers LPT-OGV test rig to validate the CFD methodology for Aero-thermal heat transfer analysis.

The work aims at numerical analysis and evaluation for two distinct scenarios by utilizing different turbulence models. The first scenario involves the on-design condition, which corresponds to the flow condition experienced by an aero-engine during

the cruise stage (Approx. AOA - 30°). The second scenario focuses on the off-design condition, which corresponds to the flow condition encountered by an aero-engine during landing/takeoff scenarios (Approx. AOA - -45°).

The study also aims to analyze the effect of the formed film coefficient over the TRS hub using CFD simulations. The obtained results are then compared against experimental data to assess the accuracy and reliability of the numerical analysis.

1.5 Objective

1. To demonstrate the capability to develop a computational model for heat transfer analysis and to understand the basics of heat transfer using CFD.
2. To build a 2d OGV computational model and evaluate it for various working conditions utilizing different turbulence models for HTC prediction. Additionally to do a thorough comparison of predicted HTC with theoretical heat transfer empirical correlations.
3. To validate the heat transfer CFD methodology by comparing with experimental heat transfer results.
4. To evaluate and study the transient effect such as wake shedding on heat transfer utilizing CFD.
5. To improve the current 1.5 stage model to incorporate purge flow addition to the CFD domain and compare it against the experimental data.

2

Theory

All the heat transfer theories are obtained from the literature [8]. All the theories for CFD are obtained from the literature [9] and [10].

2.1 Heat Transfer

Heat transfer is a domain in thermal engineering which deals with the study and analysis of the exchange of heat energy across physical systems. The heat transfer analysis mainly deals with thermal phenomena such as thermal convection, thermal radiation and thermal diffusion.

Thermal convection deals with the transfer of heat by the movement of fluids such as gases or liquids. This happens when the fluid or liquid carries thermal energy with it and circulates through the surroundings. The 2 different types of convection are forced and natural. Forced convection happens when an external force such as a fan or pump modifies the flow pattern whereas natural convection happens when the hot fluid raises and mixes with the cold fluid above.

Thermal conduction takes place in solids and stationary fluids. The transfer of heat energy takes place by the pure molecular collision of particles to transfer energy. When a material is heated, the molecular particle gains thermal energy which eventually increases the vibration energy of molecules. This vibration transfers the thermal energy to the neighbouring particles creating a chain reaction that propagates through the material.

Thermal radiation is a different form of heat transfer which does not require a medium for energy transfer. The transfer of energy happens through electromagnetic waves. The amount of thermal radiation depends on the object's temperature and its emissivity. Emissivity is the measure of an object's ability to emit infrared radiation.

These various phenomena can lead to the concentration of thermal load over the surface of the object and can eventually lead to structural failure of the object. The intensity of these thermal loads depends on the magnitude and rate of change in temperature.

2.1.1 Heat transfer coefficient

Newton's law of cooling states that, The rate of heat loss of a body is directly proportional to the difference in the temperatures between the body and its environment. The proportionality constant that is derived from this law, which relates the total surface heat flux and the temperature difference between environments is called the Heat transfer coefficient (HTC). The HTC is the ratio of total surface heat flux to the temperature difference between 2 surfaces/environments. The HTC can be mathematically expressed as:

$$h = \frac{q}{\Delta T} \tag{2.1}$$

$$\dot{Q} = hA(T_2 - T_1) \tag{2.2}$$

$$q = \frac{d\dot{Q}}{dA} \tag{2.3}$$

Where

- h = Heat Transfer Coefficient
- q = Total Surface Heat Flux
- Δ T = Change in Temperature
- Q = Rate of Heat transfer
- A = Area of surface in contact

The HTC is mainly used to measure convective heat transfer.

2.1.2 Transition

In fluid mechanics, the flow behaviour can be characterized mainly into 2 distinct regimes: Laminar and Turbulent. In the Laminar regime, the flow exhibits a smooth and predictable behaviour. This means the fluid particles move smoothly in parallel layers with little or no mixing between adjacent layers. Here the flow depicts stable and predictable behaviour. On the other hand, the turbulent regime is characterized by chaotic and irregular fluctuations in the flow. Turbulent flows are unpredictable and highly mixed due to the formation of random velocity fluctuations and swirling eddies.

Transition refers to the alteration in flow behaviour that occurs when a flow changes from a laminar regime to a turbulent regime. This transformation of flow depends on various flow factors such as Reynolds number, Velocity, Density of fluid, Viscosity of fluid, Roughness of the flowing surface and other external parameters.

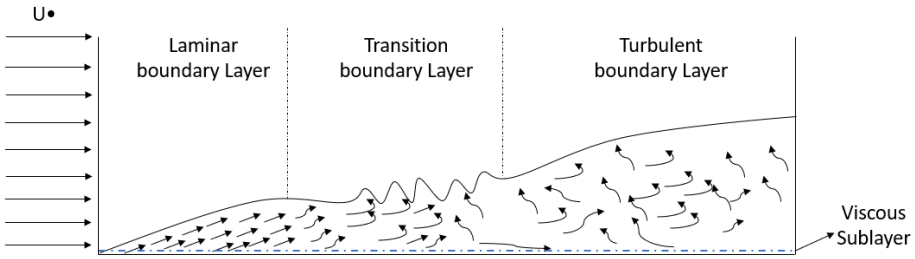

Figure 2.1: Laminar to Turbulent Trasition

The heat transfer over a domain is dependent on the flow regime. The turbulent regime enhances the heat transfer due to increased irregular fluctuations and mixing of flow. For turbulent boundary layers, the velocity gradients are high near the wall causing increased shear stress which eventually leads to an increase in heat transfer. The heat transfer in the laminar regime is low in comparison to the turbulent flow regime due to the uniform and non-mixing nature of the flow. When the transition happens, an increase in heat transfer is observed due to the laminar-turbulent transition. Therefore a thorough understanding of transition is vital for acquiring a comprehensive understanding of heat transfer occurring within a domain.

2.1.3 Dimensionless number

2.1.3.1 Reynolds Number(Re)

Reynolds number is a non-dimensional quantity that gives the ratio of inertial force to the viscous force. Mathematically Reynolds number can be represented as below:

$$\mathrm{Re} = \frac{uL}{\nu} = \frac{\rho u L}{\mu}$$

where:

- ρ is the density of the fluid (SI units: $\mathrm{kg/m^3}$)
- u is the flow speed (m/s)
- L is a characteristic Length
- μ is the dynamic viscosity of the fluid (Pa.s or $\mathrm{N \cdot s/m^2}$ or $\mathrm{kg/(m \cdot s)}$)
- v is the kinematic viscosity of the fluid ($\mathrm{m^2/s}$).

This quantity is important to characterize a flow as laminar or turbulent. For internal/pipe flows the flow becomes turbulent if the Re>3500, laminar if Re<2000 and transition if 2000<Re<3500. Whereas for an external flow, the range of Reynolds number to define a flow as laminar or turbulent varies with respect to various parameters such as the shape of the object, surface roughness etc. But in general, the flow transition happens around 10^5<Re<10^6.

2.1.3.2 Nusselt Number

Nusselt Number is a dimensionless quantity that gives the ratio of convective heat transfer to conductive heat transfer within a fluid. Mathematically representation of the Nusselt number is given below:

$$\mathrm{Nu}_L = \frac{\text{Convective heat transfer}}{\text{Conductive heat transfer}} = \frac{h}{k/L} = \frac{hL}{k}$$

where h is the convective heat transfer coefficient of the flow, L is the characteristic length, and k is the thermal conductivity of the fluid.

2.1.3.3 Prandtl Number

A prandtl number is a non-dimensional number which gives the relationship between momentum diffusivity and thermal diffusivity for a fluid.

$$\mathrm{Pr} = \frac{\nu}{\alpha} = \frac{\text{momentum diffusivity}}{\text{thermal diffusivity}} = \frac{\mu/\rho}{k/\left(c_p\rho\right)} = \frac{c_p\mu}{k}$$

where:

- ν : momentum diffusivity (kinematic viscosity)
- $\nu = \mu/\rho$, (SI units: m^2/s)
- α : thermal diffusivity, $\alpha = k/\left(\rho c_p\right)$, (SI units: m^2/s)
- μ : dynamic viscosity, (SI units: Pa s = $\mathrm{Ns/m}^2$)
- k : thermal conductivity, (SI units: $\mathrm{W}/(\mathrm{m}\cdot\mathrm{K})$)
- c_p : specific heat, (SI units: $\mathrm{J}/(\mathrm{kg}\cdot\mathrm{K})$)
- ρ : density, (SI units: $\mathrm{kg/m}^3$).

2.1.4 Empirical Correlations

2.1.4.1 Circular Cylinder Correlation

For a circular cylinder, the convection heat transfer coefficient at the stagnation point and its immediate neighbour can be calculated using the below formulation:

$$\mathrm{Nu_d} = \frac{h_c D}{k} = C\sqrt{\frac{\rho U_{\inf} D}{\mu}} \tag{2.4}$$

where:

- h_c = Heat transfer coefficient
- D = Characteristic length/diameter
- k = thermal conductivity
- C is a constant which depends on Prandtl number.
- ρ = Density
- $U_{\inf}$ = Velocity
- μ = Dynamic Viscosity

The measurement of HTC around the stagnation point is provided by the following empirical equation. This relation accurately predicts heat transfer over the leading portion of a cylinder (0deg - 80deg) and shows good agreement with experimental results [8] .

$$\mathrm{Nu}(\theta) = \frac{h_c(\theta)D}{k} = 1.14\left(\frac{\rho U_\infty D}{\mu}\right)^{0.5}\mathrm{Pr}^{0.4}\left[1-\left(\frac{\theta}{90}\right)^3\right] \tag{2.5}$$

2.1.4.2 Flat Plate Correlation

Flat plate correlation is used to estimate the heat transfer over a flat plate. This correlation serves as a basis for all the developed advanced empirical correlations. The choice of flat plate correlation depends on the flow regime, whether it is laminar or turbulent. Different correlations are used for laminar and turbulent flows because the heat transfer characteristics and flow behaviour vary significantly between these two regimes.

Laminar Flat plate correlation:

$$\mathrm{Nu_x} = 0.331\,\mathrm{Re_x}^{0.5}\,\mathrm{Pr}^{0.33} \tag{2.6}$$

Turbulent Flat plate correlation:

$$\mathrm{Nu_x} = 0.0288\,\mathrm{Re_x}^{0.8}\,\mathrm{Pr}^{0.33} \tag{2.7}$$

In this work we utilize two different methodologies to calculate the Heat transfer coefficient using empirical correlations shown in equation 2.6 and equation 2.7.

2.1.4.3 Simple Approach

In this approach, the Reynolds number is calculated using the **axial velocity** of flow and the **axial distance** to the surface of the domain. This Reynolds number is utilized to calculate the Nusselet number from which HTC is calculated.

2.1.4.4 Advanced approach

In the advanced approach, the **surface length** and **velocity just above the wall** are utilized to calculate Reynolds's Number. This provides a more accurate prediction of correlation. The velocity above the wall is calculated using Bernoulli's equation. The static and total pressure to solve Bernoulli's equation is obtained from CFD simulation.

2.2 Computational Fluid dynamics

Computational fluid dynamics is a branch of fluid mechanics which deals with numerical simulation and analysis of fluid mechanics and heat transfer phenomena. In CFD, three fundamental equations, namely the continuity equation, momentum equation, and energy equation, are simultaneously solved over the grid points/mesh

to analyze and predict the behaviour of the fluid flow. The continuity and Momentum equation for incompressible flow is given below:

Continuity Equation:

$$\frac{\partial v_i}{\partial x_i} = 0 \tag{2.8}$$

Momentum Equation:

$$\rho\frac{\partial v_i}{\partial t} + \rho\frac{\partial v_i v_j}{\partial x_j} = -\frac{\partial p}{\partial x_i} + \mu\frac{\partial^2 v_i}{\partial x_j \partial x_j} \tag{2.9}$$

The energy equation is ignored to make the theory less cumbersome.

The continuity equation corresponds to the conservation of mass, the Momentum equation corresponds to the conservation of force and the energy equation corresponds to the conservation of energy. When solving these equations, the number of unknown parameters exceeds the number of number of equations available. Hence a model is required to close these equations. A detailed description of these modelling is discussed in 2.2.1.

When the flow becomes turbulent, it shows a chaotic nature and becomes even more complex to resolve these equations. A better approach to solve this problem is to split the pressure and velocity components into a mean value and a fluctuating component. Where the mean component is the time average value of any variable and the fluctuating component is the result of chaotic behaviour of flow in turbulence.

$$v_i = \bar{v}_i + v_i' \tag{2.10}$$

$$p = \bar{p} + p' \tag{2.11}$$

$$\bar{v} = \frac{1}{2T}\int_{-T}^{T} v dt \tag{2.12}$$

Where

- $\bar{v}_i$ corresponds to the mean velocity component/time averaged component.
- v_i' corresponds to fluctuating velocity component.
- $\bar{p}$ corresponds to the mean pressure component/time averaged component.
- p' corresponds to fluctuating pressure component.

Inserting equation 2.10 and 2.11 to Continuity 2.8 and Momentum 2.9 equation. After some manipulation and solving, we obtain a new form continuity and momentum equation as shown below. This set of equations is called **Reynolds's averaged Navier stokes equation(RANS)**

RANS Continuity Equation:

$$\frac{\partial \bar{v}_i}{\partial x_i} = 0 \tag{2.13}$$

RANS Momentum Equation:

$$\rho \frac{\partial \bar{v}_i \bar{v}_j}{\partial x_j} = -\frac{\partial \bar{p}}{\partial x_i} + \frac{\partial}{\partial x_j}\left(\mu \frac{\partial \bar{v}_i}{\partial x_j} - \rho \overline{v_i' v_j'}\right) \tag{2.14}$$

Here in the RANS momentum equation 2.14, a new term ($\tau_{ij} = -\rho \overline{v_i' v_j'}$) has appeared in the diffusion term. This is an additional stress called *Reynolds Stress Tensor* which needs to be modelled.

To close/model the RANS Momentum equation, we utilize various turbulence modelling techniques. A brief description of turbulence modelling and different methodologies are given below for reference.

2.2.1 Turbulence Modelling

Turbulence modelling is a technique used in the domain of computational fluid dynamics to predict the behaviour of turbulent flow. Turbulence has a chaotic and fluctuating nature which makes the modelling of turbulence a complex process.

From equation 2.14, it is evident that a new unknown stress is formed. This unknown stress is due to the fluctuating nature of turbulent flows. Direct numerical simulation allows resolving all these fluctuating velocity components to provide a completely realistic result, but this process is computationally very expensive. Hence different methods are utilized to model these unknown stress to get a good approximation of turbulence.

In this work, k-ϵ, k-ωSST and SST Transition models are utilized to predict the heat transfer phenomena over the TRS. These models also have many inner segmentation out of which the most relevant ones for this thesis work are listed below with a brief description.

2.2.1.1 k-ϵ Model

k-ϵ model is a wildly used turbulence model to provide a statistical representation of turbulent flow field. This model solves additional equations for ***turbulent kinetic energy*** and ***turbulent dissipation rate*** coupled with conservation equations to predict the turbulent behaviour.

The Reynolds stress in equation 2.14 is modelled/closed using the Boussinesq assumption which relates Reynolds stress to the mean velocity gradient. The mathematical representation of the Boussinesq assumption is given below.

$$-\overline{v_i' v_j'} = \nu_t \left(\frac{\partial \bar{v}_i}{\partial x_j} + \frac{\partial \bar{v}_j}{\partial x_i}\right) \tag{2.15}$$

Where:

$$\nu_t = C_\mu \frac{k^2}{\varepsilon} \tag{2.16}$$

Here C_μ is a constant with a value of 0.09, k is the ***turbulent kinetic energy*** and ϵ is the ***turbulent dissipation rate***.

The modelling of Reynolds stresses introduces two additional unknowns, namely turbulent kinetic energy and turbulent dissipation rate. Consequently, a set of transport equations is defined to describe these unknowns, which can be represented as follows:

The transport equation for turbulent kinetic energy:

$$\underbrace{\frac{\partial(\rho k)}{\partial t}}_{\text{Time}} + \underbrace{\nabla \cdot (\rho \boldsymbol{U} k)}_{\text{Convection}} = \underbrace{\nabla \cdot \left[\left(\mu + \frac{\mu_t}{\sigma_k}\right) \nabla k\right]}_{\text{Diffusion}} + \underbrace{P_k + P_b - \rho\epsilon + S_k}_{\text{Sources + Sinks}} \tag{2.17}$$

where:

- P_k = Production due to mean velocity shear
- P_b = Production due to bouyancy
- S_k = Source Term

The transport equation for turbulent dissipation rate:

$$\underbrace{\frac{\partial(\rho\epsilon)}{\partial t}}_{\text{Time}} + \underbrace{\nabla \cdot (\rho \boldsymbol{U} \epsilon)}_{\text{Convection}} = \underbrace{\nabla \cdot \left[\left(\mu + \frac{\mu_t}{\sigma_\epsilon}\right) \nabla \epsilon\right]}_{\text{Diffusion}} + \underbrace{C_1 \frac{\epsilon}{k} (P_k + C_3 P_b) - C_2 \rho \frac{\epsilon^2}{k} + S_\epsilon}_{\text{Sources + Sinks}} \tag{2.18}$$

Where C1, C2 and C3 are model coefficient which varies with the type of k-ϵ model chosen. These coefficients are damped near the wall using the damping function to account for the effect of viscous dissipation near the wall.

The k-ϵ model solves equations 2.13,2.14,2.18,2.17 and 2.16 simultaneously to predict the flow behaviour.

2.2.1.2 k-ω SST Model

The k-ω model is an improved version of k-ϵ which is capable of accurately predicting the boundary layer with adverse pressure gradient. This model does not have a damping function for near-wall boundary layer prediction instead it uses a specific dissipation formulation as shown below.

$$\omega = \frac{\epsilon}{C_\mu k} \tag{2.19}$$

The k-ω model is fully capable of predicting flows with separations, divergence or shock formation. In this model, the dissipation value is dependent on turbulent kinetic energy and turbulent dissipation rate. The Transport equation is similar to the k-ϵ model, where the only difference is in the ω transport equation. The mathematical representation of the k-ω model is shown below for reference.

Turbulent Kinetic Energy(TKE):

$$\frac{\partial(\rho k)}{\partial t} + \nabla \cdot (\rho \boldsymbol{U} k) = \nabla \cdot \left(\left(\mu + \frac{\mu_t}{\sigma_k}\right) \nabla k\right) + P_k - \rho\epsilon \tag{2.20}$$

Specific Dissipation:

$$\frac{\partial(\rho\omega)}{\partial t} + \nabla \cdot (\rho \boldsymbol{U} \omega) = \nabla \cdot \left(\left(\mu + \frac{\mu_t}{\sigma_k} \right) \nabla \omega \right) + \frac{\gamma}{\nu_t} P_k - \beta \rho \omega^2 \tag{2.21}$$

The main drawback of this model is the high sensitivity to free-stream turbulence. This limitation has been successfully addressed and overcome in the k-ω SST (Shear Stress Transport) turbulence model which is independent of free-stream turbulence. This model utilizes k-ω modelling approach near the wall and a k-ϵ modelling approach away from the wall. This switch between the models is implemented using a blending function. The modified ω equation in the k-ω SST model is shown below for reference.

$$\frac{\partial(\rho\omega)}{\partial t} + \nabla \cdot (\rho \boldsymbol{U} \omega) = \nabla \cdot \left(\left(\mu + \frac{\mu_t}{\sigma_k} \right) \nabla \omega \right) + \frac{\gamma}{\nu_t} P_k - \beta \rho \omega^2 + \underbrace{2 (1 - F_1) \frac{\rho \sigma_{\omega 2}}{\omega} \nabla k : \nabla \omega}_{\text{Additional Term}} \tag{2.22}$$

Here the term F_1 servers as a blending function.

- If $F_1 = 0$ - The model behaves as a k-ϵ model
- If $F_1 = 1$ - The model behaves as a k -ω Model
- If $0 > F_1 > 1$ - The model depicts behaviour of both k-ϵ and k -ω depending on the intensity of F_1

2.2.1.3 SST Transition Model

The SST transition model is an advanced version of the k-ω SST model. This model allows the prediction of Laminar to Turbulent flow transition. This is achieved by solving 2 new transport equations in addition to the transport equations solved in the k-ω SST model. The new additional transport equations are intermittency(γ) and Momentum thickness(θ).

Where,

- The intermittency factor in the SST model represents the fraction of the flow domain where turbulence is present or active. If the γ=1 the flow is considered as fully turbulent, if γ=0 the flow is considered as fully laminar and If the γ takes values between 1 and 0, then the flow represents the transition phase.

- The momentum thickness is a parameter used to quantify the thickness of the boundary layer in a fluid flow. This quantity is used to set the smoothness of the flow transition. The mathematically representation of θ is given below:

$$\theta = \int_0^\infty \frac{\rho U}{\rho_\infty U_\infty} \left(1 - \frac{U}{U_\infty} \right) \mathrm{d}y \tag{2.23}$$

This θ is utilized to calculate a Reynolds number Re_θ at each node of the domain.

$$Re_\theta = \frac{\rho V \theta}{\nu} \tag{2.24}$$

The mathematical representation of γ transport equation is given below:

$$\frac{\partial(\rho\gamma)}{\partial t} + \nabla \cdot (\rho \boldsymbol{U}\gamma) = \nabla \cdot \left(\left(\mu + \frac{\mu_t}{\sigma_\gamma}\right)\nabla\gamma\right) + \boldsymbol{P}_\gamma - \boldsymbol{D}_\gamma \tag{2.25}$$

The $\boldsymbol{P}_\gamma$ is a function of Re_θ and are directly proportional to each other. The increase in value of Re_θ increases the $\boldsymbol{P}_\gamma$.

The mathematical representation of θ transport equation is given below:

Here we solve the equation for the transport of Re_θ

$$\frac{\partial\left(\rho\overline{Re}_{\theta,t}\right)}{\partial t} + \nabla \cdot \left(\rho \boldsymbol{U}\overline{Re}_{\theta,t}\right) = \nabla \cdot \left[\left(\mu + \frac{\mu_t}{\sigma_{\theta,t}}\right)\nabla\overline{Re}_{\theta,t}\right] + P_{\theta,t} \tag{2.26}$$

Overview of Framework:

1. Empirical value of θ is calculated to set a barrier above which transition starts.
2. The initial value of Re_θ is obtained from the specified inlet turbulence intensity.
3. γ value is set to 1, assuming the flow is fully turbulent at the start.

   The model algorithm works as shown below:
   (a) θ value at each of the nodes is calculated
   (b) Re_θ is calculated at each node and the transport equation is solved.
   (c) Re_θ value from the previous step is used to update the intermittency value in the γ transport equation.
   (d) γ transport equation is solved to find intermittency at each node(Value between 1 and 0).
   (e) This intermittency factor is used to modify the turbulent kinetic energy transport equation, allowing it to dampen or trigger the production term.
   (f) Damping the production term makes the flow laminar and triggering the production terms makes the flow fully turbulent.

2.2.2 Ansys Solver

The 2021R1 package of Ansys Fluent and Ansys CFX was employed for simulation and analysis in this work. Mesh generation was carried out using ICEM CFD 2021R1 and Fluent Meshing, and data post-processing was conducted using CFX 2021R1 Post.

2.3 Turbomachinery

2.3.1 Flow Coefficient

The flow Coefficient is a parameter that indicates the efficiency of a turbo machine. The flow coefficient is the ratio of axial velocity to the rotational speed. ie, how well the shaft rotational energy can transfer into fluid energy for a turbine. The mathematical representation of this variable is given below for reference.

$$\phi = \frac{C_a}{U} \tag{2.27}$$

All the boundary conditions are defined in terms of flow coefficient and Reynolds number. A higher value of ϕ corresponds to the high efficiency of the component and vice-versa.

2.3.2 Film Coefficient(θ)

The film Coefficient is used to predict the intensity of cold film formed over a surface. If θ takes a value of 1, this means the formed film has maximum intensity and vice-versa. Mathematically, the θ is calculated as shown below:

$$\theta = \frac{T_{Wall} - T_{air}}{T_{purgeflow} - T_{air}} \tag{2.28}$$

Where

- T_{Wall} = Wall Temperature
- T_{air} = Air Temperature
- $T_{Purgeflow}$ = Purge flow temperature

3
Methods

3.1 Geometry

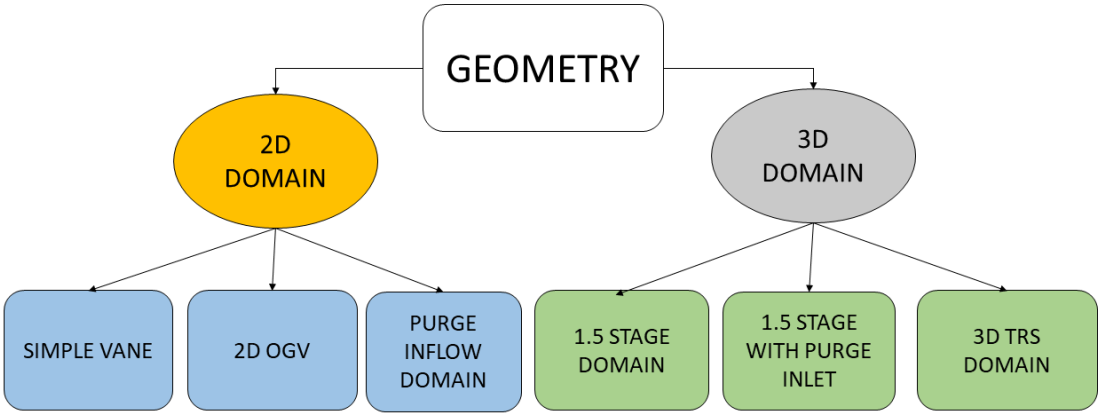

Figure 3.1: Geometry Flow Chart

In this work, 6 different geometrical models are utilized to study heat transfer over the TRS. The flow diagram shown in figure 3.1 gives a brief overview of all the models used.

3.1.1 2D Domain

3.1.1.1 Simple Vane

The model shown in figure 3.2 is used to demonstrate the capability to build and analyse heat transfer problems using Computational fluid dynamics. The geometry is a symmetric domain with a combination of semi-circular cylinders attached to a flat plate.

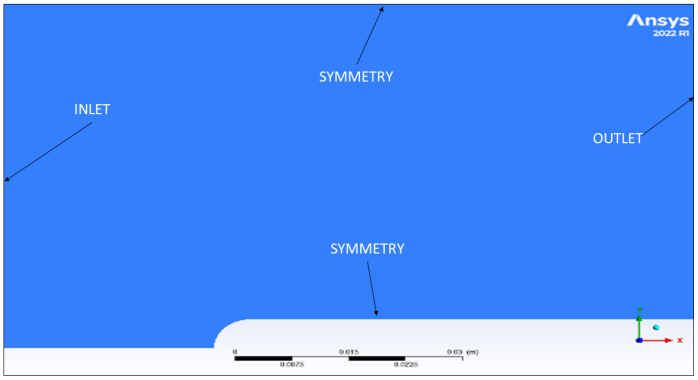

Figure 3.2: Simple Vane Geometry

3.1.1.2 2D OGV

The geometry shown in figure 3.3 is a planar cut section extracted from the 3D-OGV geometry. The 2D computational plane is extracted at the 25% vane span. This specific geometry is employed for conducting 2D analyses for various boundary conditions and cases outlined in table 3.11. By using a 2D model, there is increased flexibility and reduced computational time due to the smaller size of the mesh.

This geometrical model is evaluated for mesh Independency. The model was tested for 5 different mesh refinements of which a mesh with 64k elements is selected to perform 2D OGV analysis.

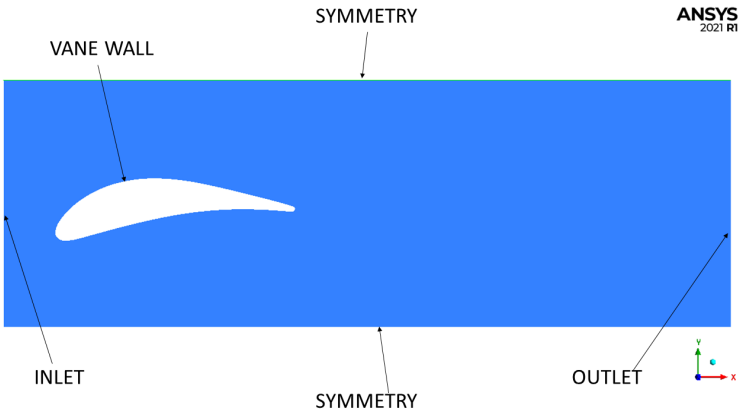

Figure 3.3: 2D OGV Domain

3.1.1.3 2D Purge Flow domain

The geometry shown in figure 3.4 is utilized to simulate the pathway through which purge flow travels towards the purge inlet. This domain corresponds to a precise cut section along the central axis of the LPT-OGV rig. The actual 2d CAD geometry of the cut section is provided for reference.

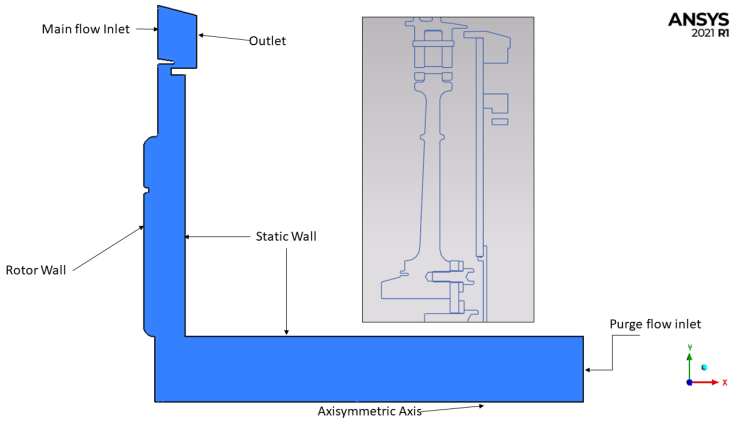

Figure 3.4: 2D Purge Inflow Domain

3.1.2 3D Domain

3.1.2.1 1.5 Stage domain

The Geometry shown in figure 3.5 is the front view of the entire 1.5-stage computational domain used for all the analysis. This model consists of a single periodic section of an annular geometry, consisting of a 6° stator, a 5° rotor, and a 30° of OGV segments. The actual experimental setup consists of a rotor domain with 72 blades, a stator domain with 60 blades and the TRS domain with 12 blades.

Running the simulation for a full annular geometry would result in increased mesh size which requires huge computational time. This is the reason to use a single periodic segment of the rotor, stator and OGV blade for analysis.

This computational domain is validated by GKN Aerospace specifically for analysis and simulation, and it is exclusively intended for CFX analysis. The stator, rotor, and OGV domains are interconnected using an interface plane. Prior to this work, GKN has already conducted mesh validation and mesh independence tests, confirming that this model is ready for direct use in simulations and analysis[7].

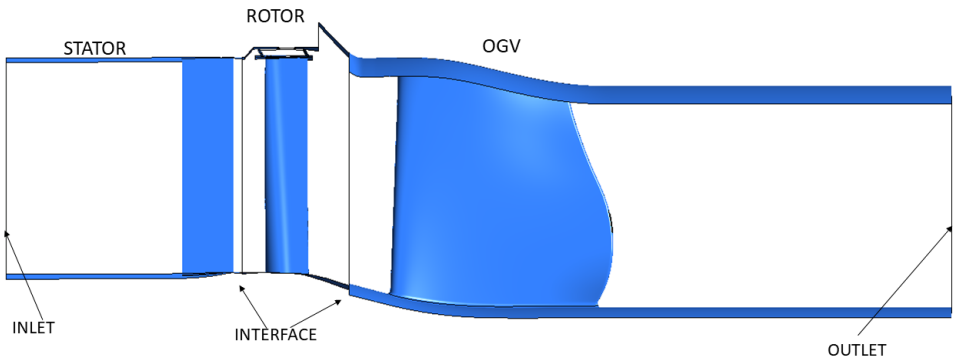

Figure 3.5: 1.5 Stage Geometry

3.1.2.2 1.5 Stage with Purge inlet

To implement the purge flow addition, a new model is developed by modifying the 1.5-stage computational domain discussed in section 3.1.2.1. The modification is done in the rotor domain of the 1.5-stage model. This modification replicates the actual purge pocket in the experimental setup. The geometrical modification is done using NX Siemens software. The purge 1.5 stage computational domain is shown in figure 3.6 for reference.

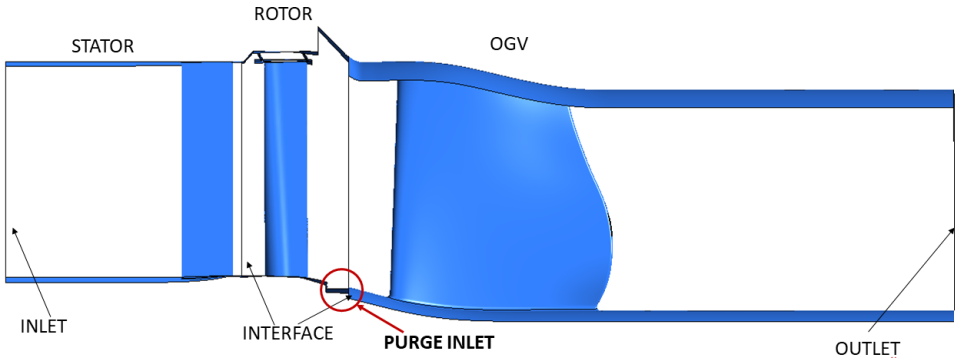

Figure 3.6: 1.5 Stage Geometry with Purge modification

A detailed picturisation of the rotor domain with and without purge modification is shown in figure 3.7 for better clarification. The purge inlet is where the purge mass flow is defined as a boundary condition, this surface is nothing but the cavity between the rotor hub and the TRS hub.

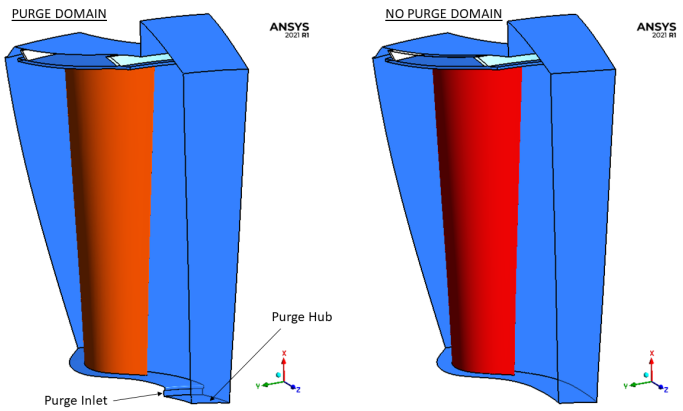

Figure 3.7: 1.5 Stage Geometry - Only Rotor domain

3.1.2.3 The TRS domain

This thesis primarily focuses on conducting an analysis of heat transfer concerning the geometry of the TRS. The geometry shown in figure 3.8 corresponds to the computational domain with only the TRS segment. This domain is utilized to obtain a more accurate heat transfer result.

This domain is a periodic section of TRS. The domain corresponds to a 30°segment of the TRS domain.

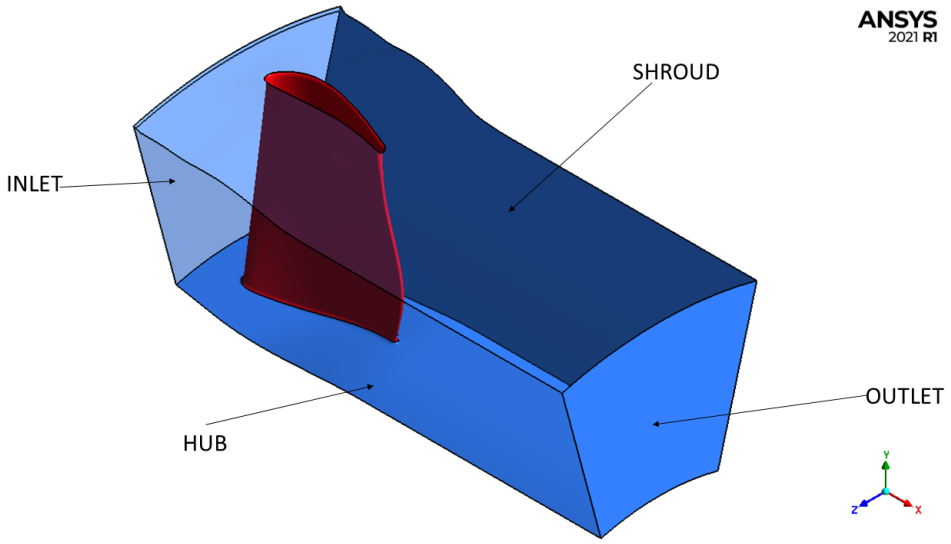

Figure 3.8: TRS Computational flow domain

3.2 Mesh

This paper utilizes the geometrical models mentioned in section 3.1 for analysis and simulation. The 1.5 stage model and the Only OGV model are directly utilized without conducting additional analysis, such as mesh Independence studies. Prior to this work, these computational models have been extensively used and previously validated by GKN for simulation and analysis purposes ([6],[7]).

3.2.1 2D Mesh

All 2D simulation models mentioned in Section 3.1 have undergone a mesh independency test to ensure a high-quality mesh with good wall y+ values. The mesh consists of 54,000 elements, with 1st layer thickness of 5e-6[m]. The growth is set to 1.1, encompassing a total of 24 layers. A smooth transition is maintained across the entire 2D domain, and the maximum y+ value is limited to 0.4. This mesh quality guarantees reliable results for thermal analysis.

3.2.2 3D Mesh

In this study, the mesh and geometric model for 3D analysis, excluding the purge 1.5 stage domain, were provided by GKN Aerospace. Specifically, the focus of this research is on the development of a mesh for the rotor segment of the 1.5-stage domain with purge modification. The developed mesh adheres to the same mesh size, wall refinements, growth rate, and y+ values as the original conventional mesh provided by GKN.

For the endwalls, the first layer thickness is set to 2e-5[m] with a growth rate of 1.2, resulting in 34 layers. In the case of the vane, the first layer thickness is set to 1e-5[m] with a growth rate of 1.2, and there are a total of 32 layers.

The modified geometry was meshed using Ansys 2021R1 ICEM CFD, employing a fully structured hexahedral mesh. The current mesh quality ensures a maximum y+ of 0.9 near the end walls and vane. This wall refinement has been applied to ensure the suitability of the mesh for heat transfer analysis.

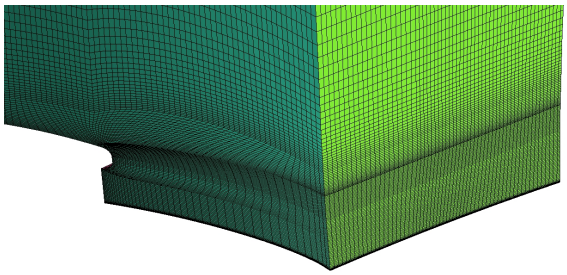

Figure 3.9: Rotor Mesh with Purge Modification

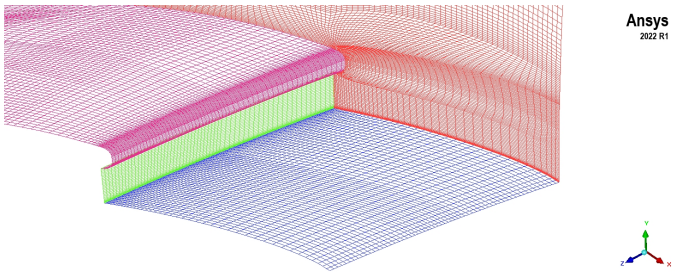

Figure 3.10: Rotor Mesh with Purge Modification - Wired Frame

3.2.3 3D representative 2D mesh

To facilitate a comparative analysis between 2D and 3D simulations, a 2D mesh was created to serve as a representative of the 3D geometry. This 2D mesh was designed to replicate a cross-sectional plane at a 25% span of the 3D mesh. The 25% span 3D section consisted of approximately 45,000 elements, while the developed 2D has approximately 50,000 elements. The 2D mesh was developed with the same level of refinement, first-layer thickness, and y+ values as those specified for the 3D mesh in the previous section. This mesh is used to compare the analysis results between 2D and 3D mesh.

3.3 Boundary conditions

The primary objective of this thesis is to utilize the available heat transfer experimental data from the Chalmers LPT-OGV test rig to validate the CFD methodology for Aero-thermal heat transfer analysis.

The On-design condition corresponds to the engine's operating condition during the cruise stage(approx AOA 30°), while the Off-design condition represents the working condition during landing and take-off scenarios(approx AOA +-45°). The analysis primarily focuses on these two cases due to the high probability of aero engines being subjected to these working conditions. Understanding the heat transfer processes occurring under these conditions is crucial for comprehensive analysis.

This work focuses on utilizing 3 different turbulence models for analysis and comparison, namely k-ω SST, k-ϵ and the SST Transition model. The k-ω SST and k-ϵ are fully turbulent models and the SST transition model is a transition model capable of capturing the transition effects.

The analysis without purge utilizes the computational domain described in section 3.1.2.1 and 3.1.2.3. The analysis which involves purge flow utilizes the computational domain described in sections 3.1.2.2 and 3.1.2.3. The table 3.11 gives the boundary conditions for which the simulations are carried out. The required mass flow rate is defined at the stator inlet and purge inlet. The required RPM is defined at the rotor domain to run the 1.5-stage model.

TYPE	Analysis	Turbulence model	Reynolds Number	Inlet Mass Flow[Kg/s]	Flow Coeffecient	RPM(Rev/min)	Purge Mass Flow[Kg{s]	Inlet Temperature[K]	Wall Temperature[K]	Purge Temperature[k]
Without Purge	On design	k-ε Standard Model	350000	17.85	0.622	832	_	288.24	293.24	_
		k-ω SST Model	350000	17.85	0.622	832	_	288.24	293.24	_
		SST Transition Model	350000	17.85	0.622	832	_	288.24	293.24	_
Without Purge	Off Design	k-ε Standard Model	350000	17.84	0.355	1491	_	288.24	293.24	_
		k-ω SST Model	350000	17.84	0.355	1491	_	288.24	293.24	_
		SST Transition Model	350000	17.84	0.355	1491	_	288.24	293.24	_
With Purge	On design	SST Transition Model	350000	17.85	0.622	832	0.1785	290	Adiabatic Wall	280
With Purge	Off Design	SST Transition Model	100000	5.06	0.355	424	0.0506	290	Adiabatic Wall	280

Figure 3.11: Table - Boundary Conditions

The reference pressure is set to ambient condition for all the simulations(i.e. P = 101325[Pa]). The OGV domain walls(Hub, Shroud and Vane) are set to wall temperature and inlet flow is set to inlet flow temperature for non-adiabatic simulations. For the case with purge flow, all the wall is set as an adiabatic wall. The inlet temperature and purge inlet temperature are set accordingly to analyse the film coefficient.

3.4 Measurement Planes - Experimental Data

The experimental data are limited to a specific surface area within the TRS domain, as shown in Figures 3.12, 3.13, 3.14 and 3.15. The comparison between numerical simulation and experimental measurements is performed exclusively within this region. The highlighted green area represents the region where experimental data is available.

For detailed analysis poly-lines are defined over the surface of hub, shroud and vane region as shown in the following figures.Comparison plots between experimental measurements and numerical analysis are obtained over these defined lines.

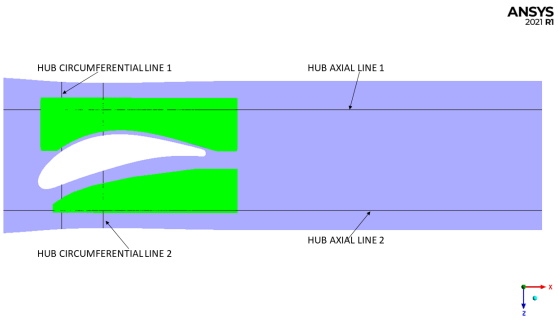

Figure 3.12: Hub side view - TRS

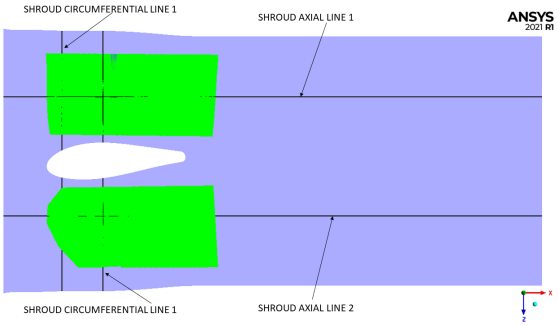

Figure 3.13: Shroud side view - TRS

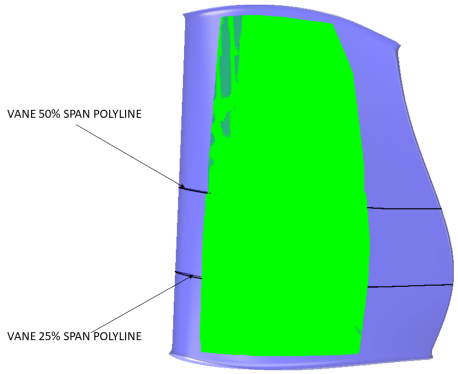

Figure 3.14: Pressure side view

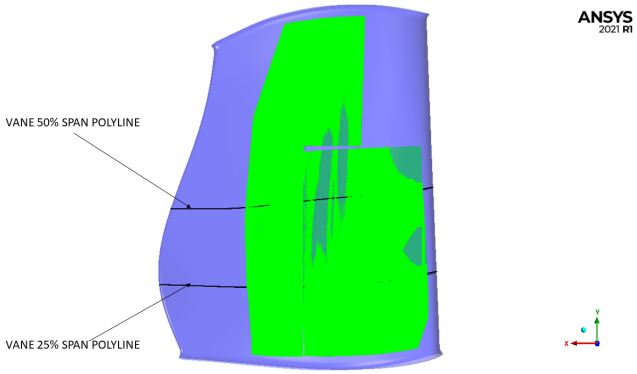

Figure 3.15: Suction side view

3.5 Analysis

The main focus of this study is the steady-state analysis of TRS heat transfer. However, for extreme off-design cases, transient analysis is conducted to examine the transient effects on end-wall heat transfer of TRS.

3.5.1 Experimental Data

The experimental heat transfer data utilized in this study for CFD method validation is obtained from Chalmers LPT-OGV test rig facility. This dataset encompasses information related to both on-design and off-design analyses, as well as on-design and off-design analyses with the inclusion of purge flow. Specifically, the data consists of temperature values along with their corresponding x, y, and z coordinate values. Additionally, the dataset includes film coefficient values across the HUB surface.

3.5.2 2D analysis

The computational model discussed in section 3.1.1.1 is utilized to understand basic heat transfer phenomena. Here the comparison with empirical correlation, the effect of Reynolds number and the effect of temperature on heat transfer is studied.

The computational model discussed in section 3.1.1.2 is utilized to evaluate heat transfer over a plane located at 25% spanwise distance of OGV. Here, all the analysis is carried out in the Ansys Fluent module, utilizing all the 3 turbulence models mentioned in section 2.2.1. All the 2D analysis is set to have an inlet turbulence intensity of 5% and turbulence length scale of 0.0012[m]. A comprehensive comparison is conducted to evaluate the CFD results obtained from three different turbulence models. Furthermore, a comparison is made between the CFD results and the empirical correlation for heat transfer. Additionally, the 2D results are compared to the 3D results to further analyze the differences between them.

The computational model described in section 3.1.1.3 is employed to simulate the flow pathway of the purge flow, starting from the purge main inlet and progressing towards the cavity between the rotor hub and the OGV domain.The primary goal of this analysis is to assess the velocity component at the entrance of the cavity located between the rotor hub and the OGV domain. Here an axisymmetric swirl configuration is used for the analysis.

3.5.3 3D Analysis

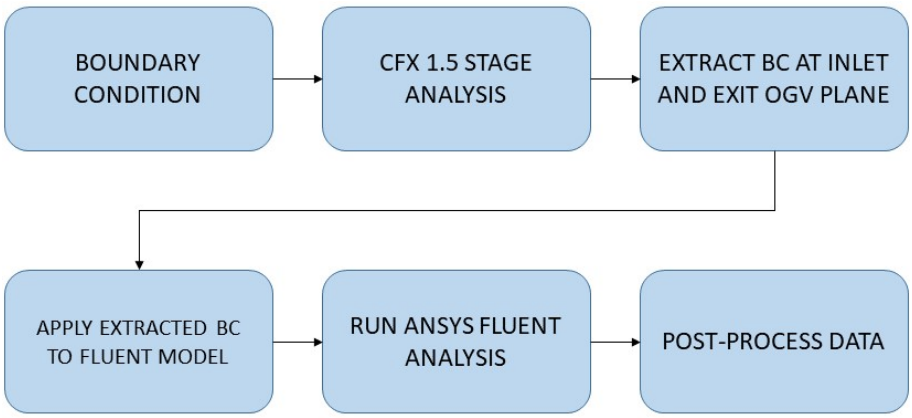

Figure 3.16: Analysis Frame Work

In this work, the 3D analysis is divided into 2 segments, The first one is the 1.5-stage ANSYS CFX analysis and the second is the ANSYS Fluent analysis with only the TRS domain. The purpose of the 1.5 Stage analysis is to extract boundary data such as axial velocity, radial velocity, circumferential velocity, temperature and turbulent quantities at the inlet and exit planes of the TRS domain. Figure 3.17 provides a visual representation of these extraction planes. The extracted boundary data are applied to ANSYS fluent solver as boundary profile data to evaluate TRS heat transfer in detail using the TRS model.

The Ansys CFX analysis utilizes Shear Stress Transport(SST model) for modelling turbulence. This model is the same as k-ω SST model discussed in section 2.2.1.2, but optimized for CFX solver. From experimental results, the flow over the OGV

surface is observed to have transition effects. One of the primary objectives of this work is to determine the most suitable turbulence model for evaluating heat transfer over the OGV domain. For this purpose, Ansys fluent simulation utilizes a fully turbulent model(k-ω SST Model) and a transition model(SST Transition Model) for heat transfer analysis.All the 3D analysis is set to have an inlet turbulence intensity of 5% and turbulence length scale of 0.0012[m].

The Framework of 3D analysis is given in figure 3.16 for reference and explained below.

1. The given boundary condition shown in table 3.11 is applied to the 1.5-stage CFX model.
2. The 1.5 stage analysis utilizes the model discussed in sections 3.1.2.2 or 3.1.2.1 for analysis according to the boundary conditions applied.
3. The results of the converged 1.5 stage analysis are used to extract radial averaged boundary profiles at the OGV inlet plane and exit plane.
4. This extracted boundary data is applied to the Only OGV domain model discussed in section 3.1.2.3. The Ansys Fluent is used to run this analysis with the required turbulence model.
5. Results from Ansys Fluent simulation are post-processed using Ansys CFX post.

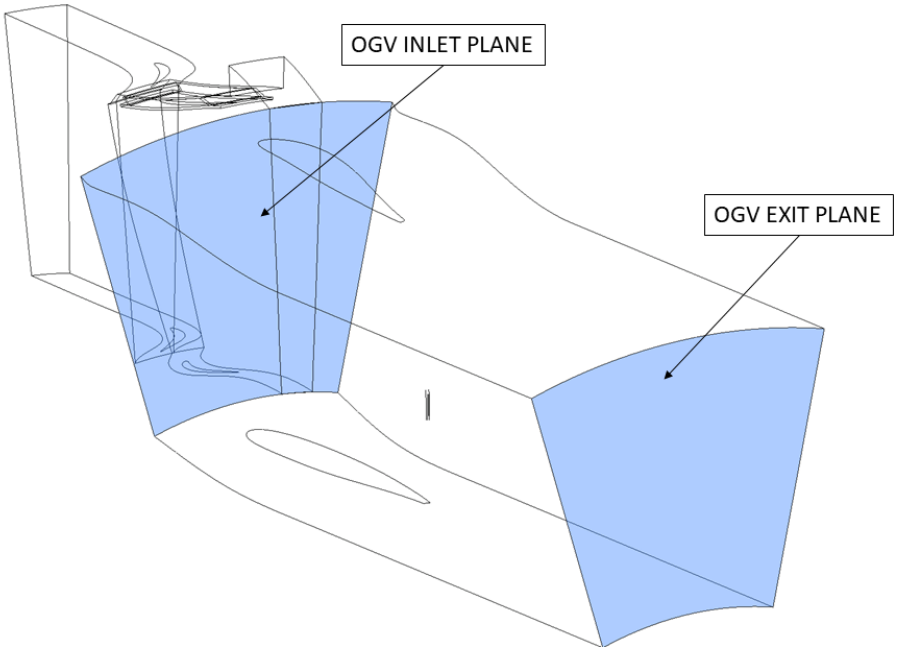

Figure 3.17: Boundary data extraction plane

4

Results

4.1 Simple Vane

The simple vane analysis is evaluated to develop a good understanding of heat transfer analysis. Figure 4.1 shows the velocity contour plot superimposed to HTC correlation and CFD predicted HTC.

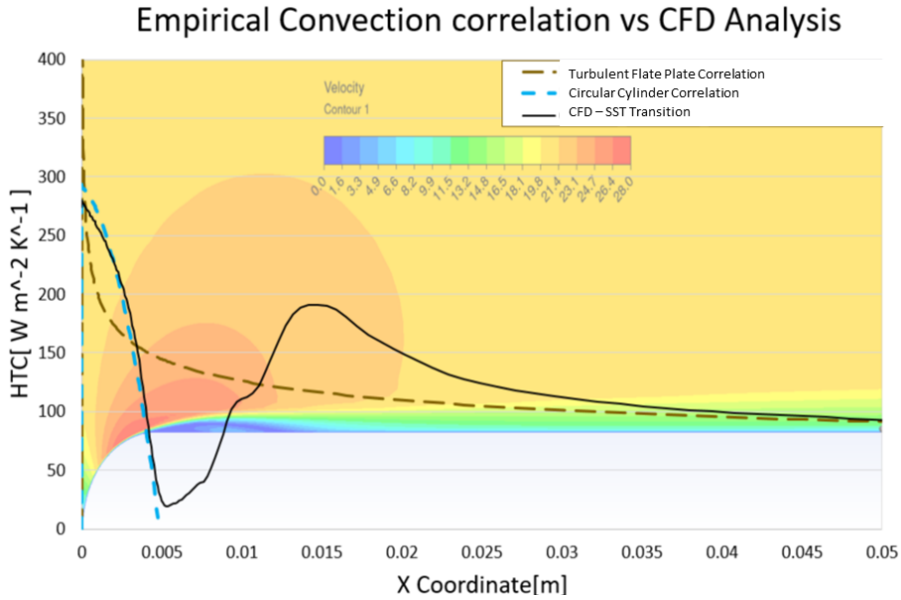

Figure 4.1: A comparison between heat transfer correlations and CFD results from the simple vane analysis

Based on the velocity contour, it can be observed that the flow detaches from the surface of the simple vane due to its curvature, resulting in a small separation. However, towards the aft, a noticeable reattachment of flow is visible. The predicted HTC from heat transfer correlation for the cylinder is plotted using the equation 2.5 and the turbulent flat plate correlation is plotted using equation 2.7.

When air flows over the simple vane, the flow at the leading edge is fully turbulent, resulting in effective air mixing and increased convective heat transfer. However, as the flow progresses along the surface of the OGV, a laminar boundary layer forms, which reduces convective heat transfer. This reduction continues until the laminar boundary layer becomes unstable and undergoes transition due to an increase in flow velocity caused by the curvature of the simple vane. When the transition occurs, the

flow becomes more chaotic, resulting in enhanced mixing between the airflow and the surface of the OGV. This increased mixing contributes to improved convective heat transfer in the transition regime. Eventually, the flow fully transitions to a turbulent state, further boosting the heat transfer. These phenomena are clearly illustrated in Figure 4.1.

From figure 4.1, it is observed that the predicted HTC using cylindrical heat transfer correlation and the CFD results agree well at the leading edge and the region around it. Towards the aft of the simple vane, the CFD results agree well with the turbulent flat plate correlation. In general, from the simple vane analysis, the HTC prediction at the leading edge of the circular cylinder is accurately predicted by empirical correlations and it is validated by comparing it with CFD results. Additionally, when the transition occurs, and an increase in HTC is also observed.

4.2 2D OGV Vane

4.2.1 On-design

The velocity contour of flow over the 2D OGV for the on-design case is given in figure 4.2. The computational domain is simulated using 3 different turbulence models(i.e. k-ϵ Standard, k-ω SST, and SST Transition.). The velocity contour shown in figure 4.2 represents the result from SST Transition analysis. Refer to Appendix A.0.1 for contour plots on other turbulence models. Figure 4.3 shows the comparison of HTC predicted by empirical correlations, CFD models and experimental data. The plot is segmented into Suction-side data and Pressure-side data. The turbulent and laminar empirical correlation is calculated using the method described in 2.1.4.4 which is compared against experimental data extracted at the 25% span of OGV Vane.

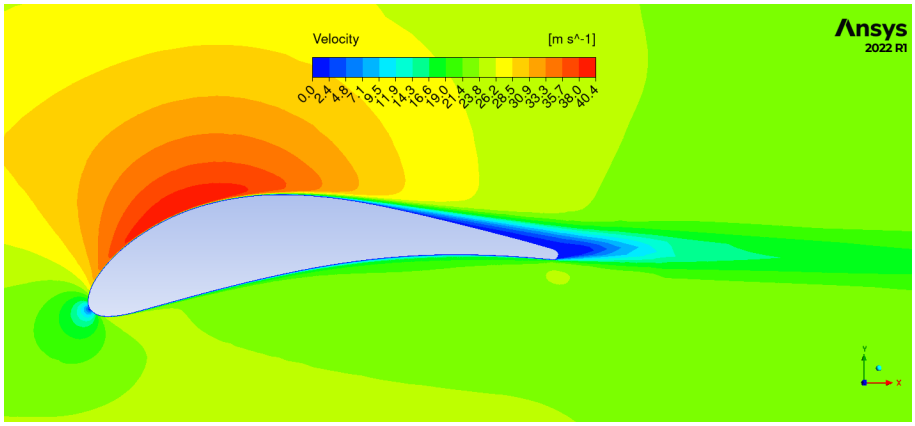

Figure 4.2: Velocity contour from on-design analysis simulated using SST transition turbulence model

4.2.1.1 Suction Side

As discussed in section 4.1, a similar profile of HTC is observed at the suction side of 2D vane. The HTC results from CFD analysis predicted by different models fall within the range predicted from empirical correlations for turbulent flat plate and laminar flat plate. Comparing the heat transfer profile with experimental data, it is observed that the SST Transition model exhibits a similar trend. The model successfully captures the transition effect, indicating its capability in simulating the transitional flow regime. However, the SST Transition model under-predicts the experimental results and an earlier transition is observed in CFD results.

In the k-ω SST model, the transition phenomena are not captured. The flow regime predicted by this model tends more towards a turbulent regime. The k-ϵ model mostly aligns with the profile of the turbulent correlation across the entire OGV boundary, which makes this model the least accurate model for HTC prediction. Towards the aft, an increase in heat transfer is observed on the k-ω SST model and SST Transition model. This is due to the increased circulation/flow detachment towards the aft.

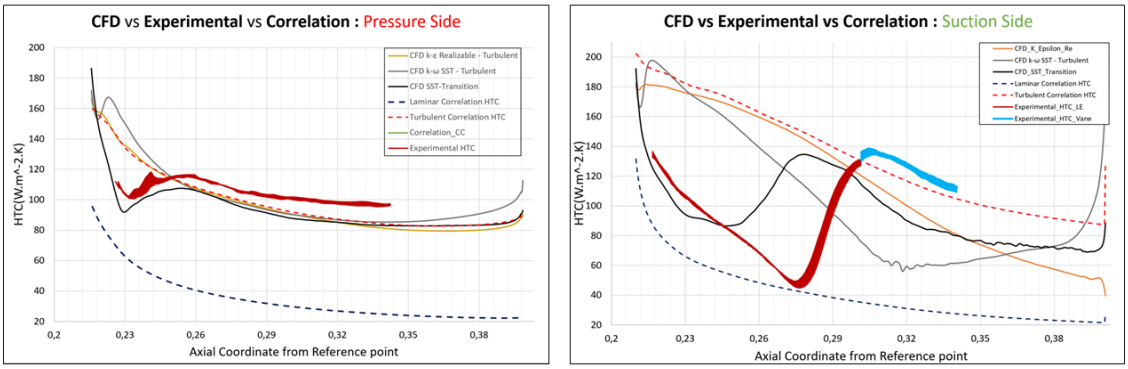

Figure 4.3: HTC comparison between heat transfer correlations, experimental data and CFD analysis

4.2.1.2 Pressure Side

Similar to the suction side, the inference holds true for the pressure side as well. As the previous case, the SST Transition model provides more accurate predictions of the HTC compared to other turbulence models. The CFD-predicted values for HTC on the pressure side fall within the range between the laminar and turbulent correlations. Towards aft all the models follow the turbulent correlation.

4.2.2 Off-Design

For the off-design analysis of the 2D OGV, similar conclusions were drawn. However, notable differences were observed on the pressure side. A higher AOA led to increased separation of the flow, resulting in the formation of a large wake. This separation caused a substantial increase in the HTC due to the presence of reverse

flow within the wake. Towards the aft, on the suction side, a shift in the stagnation point and transition is observed. All the reference contours and plots are added to Appendix A.0.1.

4.2.3 2D Analysis Vs 3D Analysis

A comparative analysis was conducted to examine the distinctions between 2D and 3D analyses. To facilitate this, a 2D mesh was generated with a level of refinement matching that of a 3D section plane at 25% of the vane span. Both meshes had identical wall refinement and mesh quality. The HTC results obtained from the 2D and 3D analyses were then compared with experimental data, as depicted in Figure 4.4.

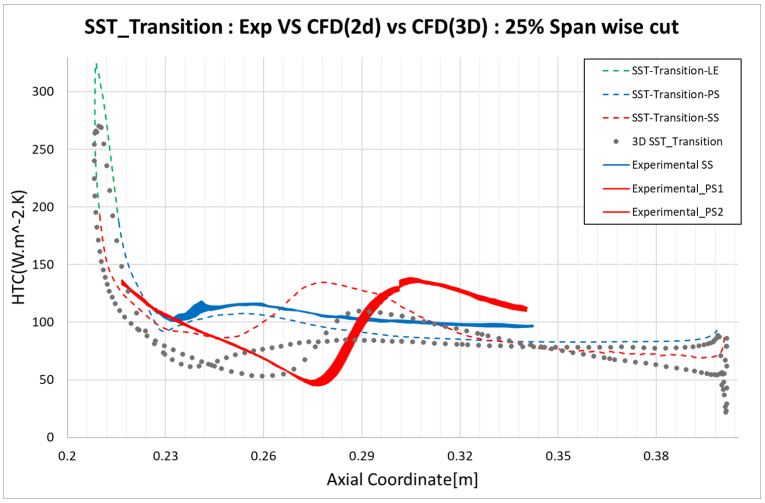

Figure 4.4: HTC over 25% span for on design - A comparison with 2D CFD, 3D CFD and Experimental results

The findings reveal a noticeable difference between the predicted HTC values in the 2D and 3D simulations. This difference can likely be attributed to the three-dimensional flow effects upstream and the simplification inherent in the linear cascade assumption made in the 2D analysis. Upon closer examination of the results on the suction side of vane, it becomes evident that the 3D predictions are in closer agreement with the experimental data. Unfortunately, it is challenging to draw a conclusive comparison at the leading edge of the vane due to the unavailability of experimental data at the 25% span of the vane.

4.3 3D On-design

In this work, The 3D on-design data for all the turbulence models is already provided by GKN Aerospace. For the On-Design case, this work focuses on post-processing the data for detailed conclusions. Figure 4.5 shows the HTC contour over the surface of the TRS structure. The main area of focus is the Hub, Shroud, and Vane region of TRS. The on-design simulation is carried out using a fully turbulent model(k-ω

SST) and a transition model(SST Transition Model). The CFD results are compared against the experimental data as shown in figure 4.5.

The experimental data is post-processed as contour data using Ansys CFX-Post software. The import surface data feature in Ansys CFX-Post is utilized to plot the experimental contour data. All the contour data shown in figure 4.5 is plotted for the same colour scale and the max and min value of HTC is limited to 180 [Wm^2K^{-1}] and 40 [Wm^2K^{-1}] for a clear picturisation.

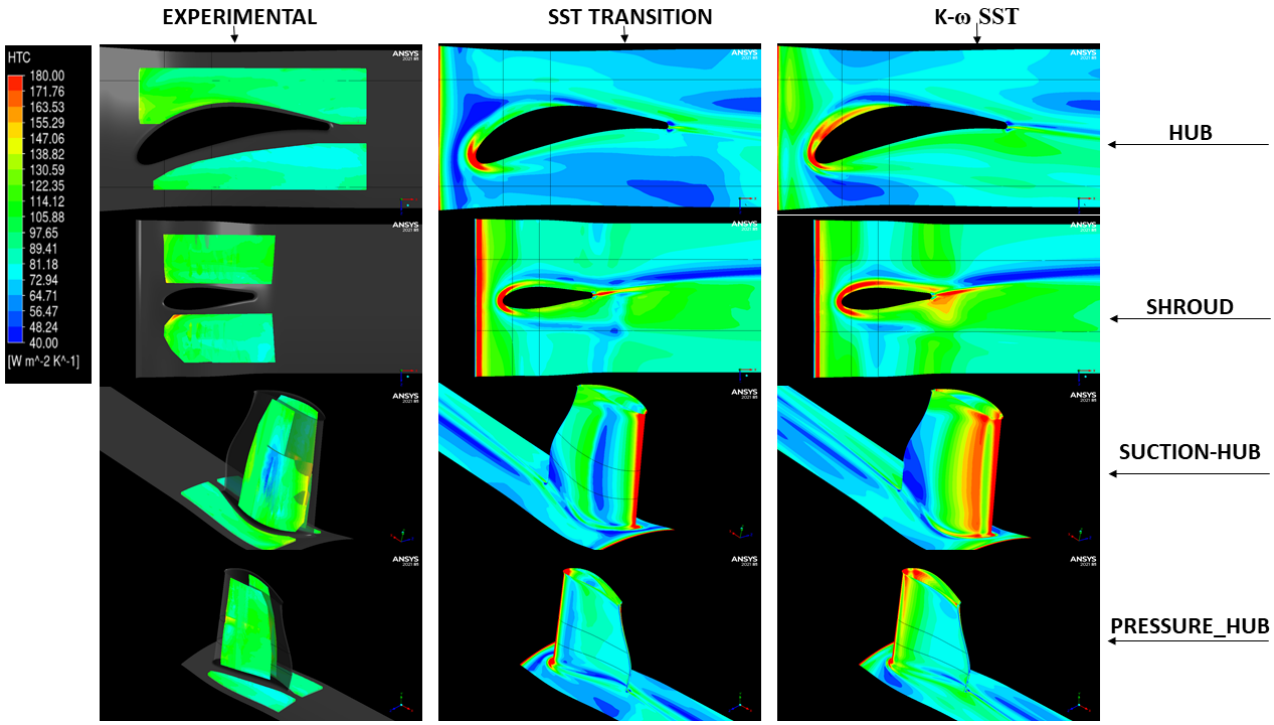

Figure 4.5: HTC contour - On Design Results

4.3.1 Vane Suction Side

In figure 4.5, the suction-hub HTC contour shows the heat transfer over the suction side of the vane. The experimental contour clearly indicates that the flow undergoes transition at around 30% of the vane's axial length. This transition behaviour is accurately captured by the SST Transition model. However, the k-ω SST model fails to capture this effect, where this model predicts a higher heat transfer. Additionally, it is worth noting that the transition behaviour remains consistent throughout the span of the vane.

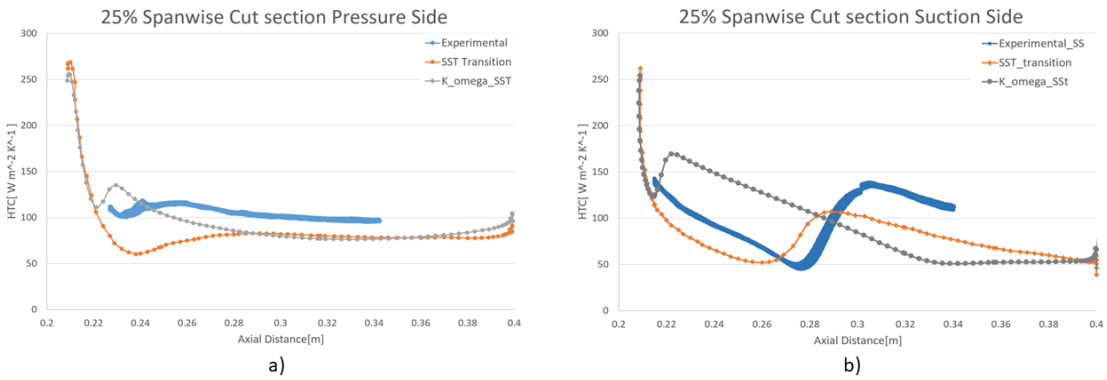

Figure 4.6: HTC | Comparison with Experimental and CFD results | 25% Span wise section plane

A more detailed interpretation can be obtained from the HTC over the polylines discussed in section 3.4. The measured HTC data over the polyline defined at 25% vane span for experimental and CFD is given in figure 4.6. From the figure 4.6**(b)**, it is evident that the SST transition model predicts the same profile as experimental data, but with an earlier transition. As observed in 2D simulation results, the SST Transition CFD results under-predict the convective heat transfer. The k-ω SST model shows a full turbulent behaviour where the predicted heat transfer values are not similar to experimental data.

4.3.2 Vane Pressure Side

The pressure-hub HTC contour in figure 4.5 shows a small transition happening on the vane pressure side. This transition effect is captured by the SST Transition model. Towards the aft, both SST Transition and k-ω SST model predict similar HTC. Same as the suction side, SST transition under-predicts the HTC when compared with experimental results. In Figure 4.6**(a)**, the results are shown for the pressure side along the polyline located at 25% of the vane span. These results align with the previous observations made regarding the contour results.

In general, the SST transition model is capable of predicting the same HTC profile as experimental data. Although, the model under-predicts the HTC and predicts an earlier transition when compared with experimental results. The k-ω model is not suitable for accurately predicting heat transfer over the vane when the flow exhibits transition behaviour. This model is more appropriate for cases where the flow remains fully turbulent.

4.3.3 Hub

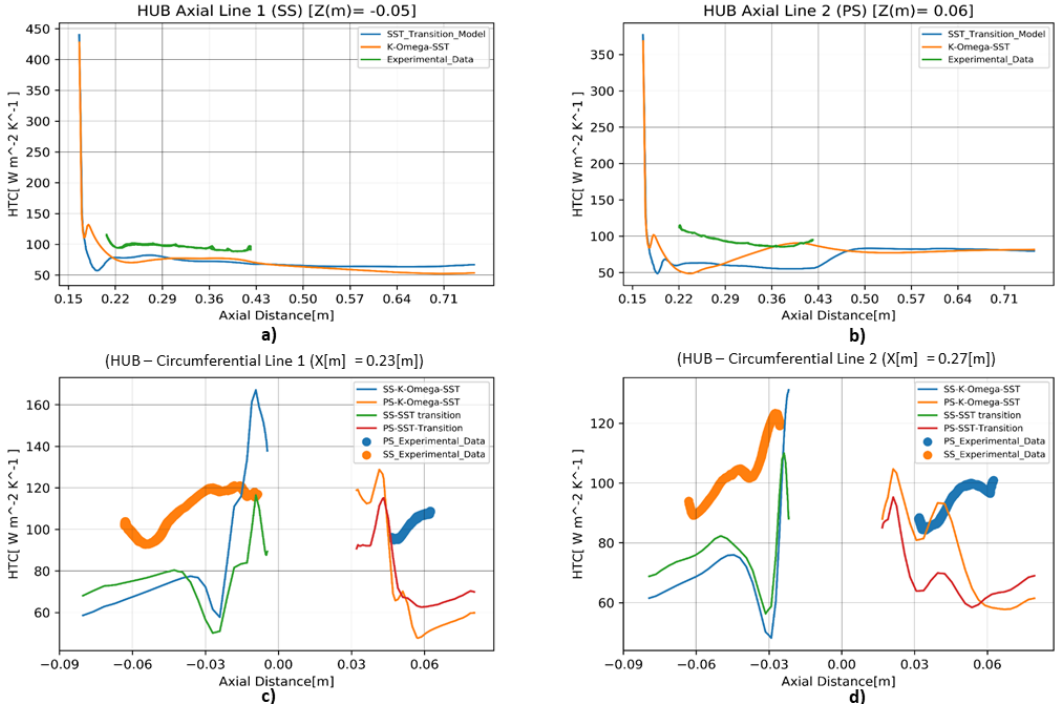

Figure 4.7: HTC HUB - Experimental vs CFD comparison over the defined polylines

Figure 4.7 shows the measured HTC over the hub polylines defined in section 3.4. The figure shows the comparison between experimental, k-ω SST and SST transition results. From the contour shown in figure 4.5 for Hub, an increased heat transfer is observed over the OGV leading edge-fillet region. This is due to the formation of a horseshoe vortex at this region. A greater heat transfer is observed near the hub fillet according to the CFD results, although there is a lack of experimental data in this specific region.

A detailed comparison is observed from the figure 4.7. Here for the HUB axial line 1 and 2, we see the same observation discussed in the previous section for CFD results. The SST Transition model shows a similar profile to the experimental data in terms of HTC, although it tends to underestimate the actual values.

When examining the HUB Circumferential lines 1 and 2, we observe that the CFD models under-predict the HTC values compared to the experimental data as we move away from the OGV. Near the vane, the CFD models over-predict the HTC values. However, it is important to note that the unavailability of experimental results near the OGV fillet prevents a definitive conclusion. In addition to these observations, both the turbulence model shows increased variations in predicted HTC when compared with experimental data.

4.3.4 Shroud

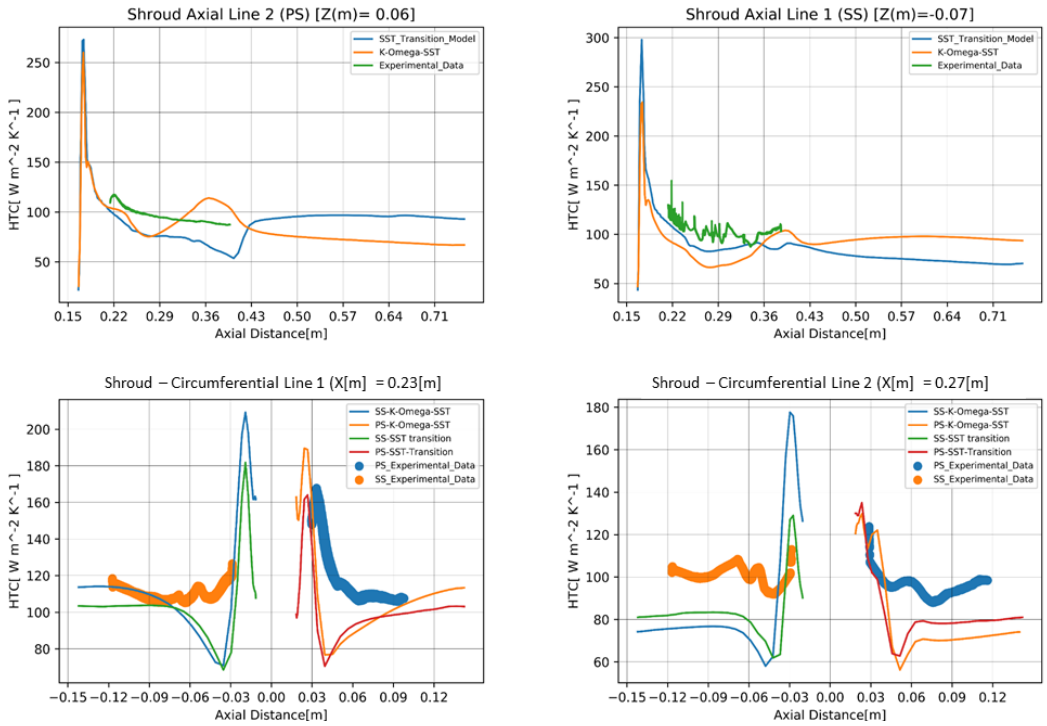

Figure 4.8: HTC SHROUD - Experimental vs CFD comparison over the defined polylines

Figure 4.8 shows the measured HTC over the shroud polylines defined in section 3.4. The HTC contour of the Shroud indicates increased heat transfer near the OGV leading edge side due to the formation of a horseshoe vortex. Similarly, the inlet of the shroud shows higher heat transfer due to flow re-circulation inside the pocket before reaching the shroud surface. Evaluating the results shown in figure 4.8 gives the same inferences as the results discussed in section 4.3.3.

In general, for on-design analysis, the SST Transition model exhibits a similar profile to the experimental data. However, it consistently underpredicts the experimental values. On the other hand, the k-ω model does not match the experimental data, except in regions where the flow is expected to be fully turbulent, where it provides accurate predictions.

An increased HTC is predicted by the CFD simulations near the OGV fillets. However, due to the absence of experimental data in this particular region, the significance of this observation remains unclear. Notably, both the hub and shroud surfaces exhibit high fluctuations in CFD heat transfer predictions. Additionally, an increased HTC is observed near the hub leading edge and shroud leading edge due to the formation of a horseshoe vortex.

4.4 Off-Design Analysis

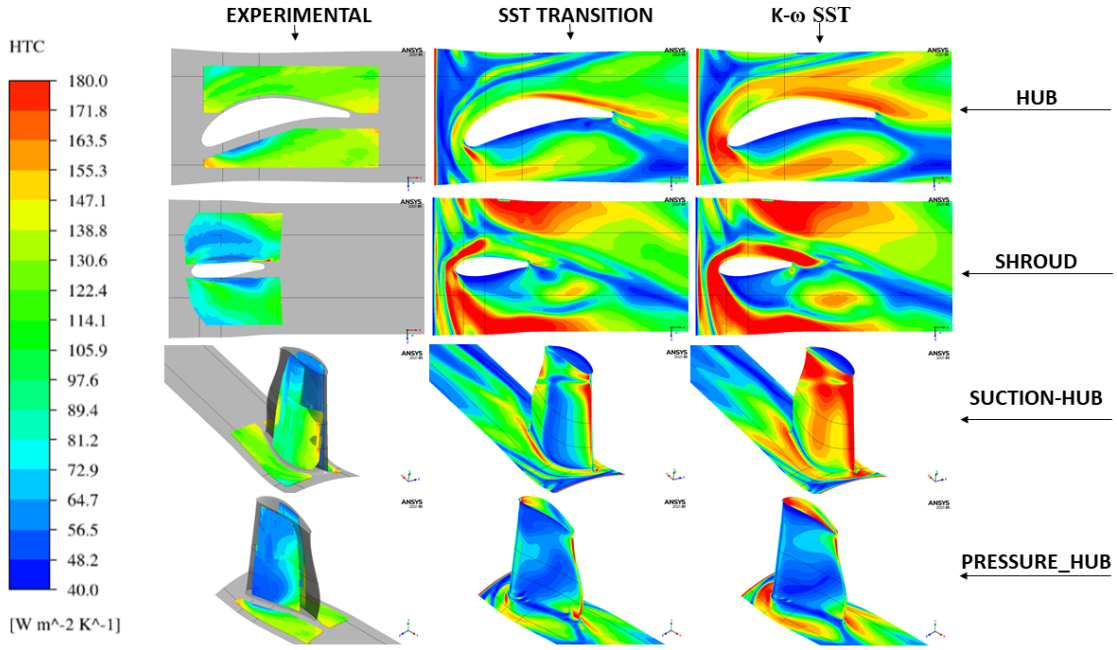

Figure 4.9: HTC Contour - Off Design Analysis

A comprehensive off-design analysis was conducted as part of this work, involving the utilization of the 1.5-stage model to extract boundary conditions at the TRS inlet plane and TRS exit plane. The only TRS model was used to simulate the off-design boundary conditions, employing the SST Transition model and the k-ω SST model. The experimental data are posted as contour results utilizing the Ansys CFX import surface data feature. The heat transfer contour from all the off-design CFD analysis and experimental results are given in figure 4.9.

4.4.1 Vane Suction Side

The contour plots of experimental and SST transition CFD resutls clearly indicate a noticeable change in the flow transition on the vane's suction side. In the case of off-design conditions, where the angle of attack is higher, the transition point is observed to shift towards the aft. This shift is primarily attributed to the higher angle of attack, which causes the stagnation point of the flow to move towards the aft direction. Consequently, the flow experiences a greater acceleration, resulting in the transition being shifted towards the aft region of the vane.

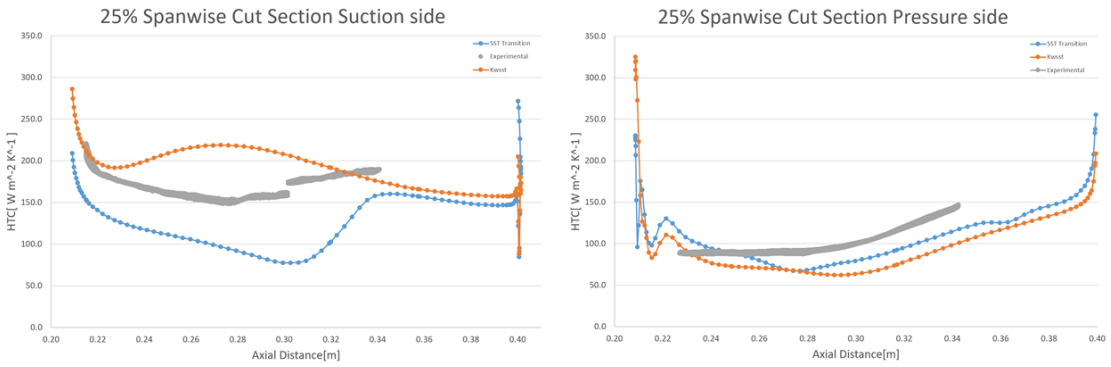

Figure 4.10: HTC | Comparison with Experimental and CFD results | 25% Span wise section plane

The HTC plots shown in Figure 4.10 allow for a comprehensive interpretation of the observations. Specifically, Plot (a) illustrates the suction side data of a polyline defined at 25% span of the vane. Analysis of this plot reveals that the experimental results fall within the range of predictions made by the SST transition model and the k-ω SST model. However, it is worth noting that the SST transition model underestimates the experimental values. Furthermore, the experimental data demonstrates that the transition occurs over a longer duration than what the SST transition model predicts.

4.4.2 Vane Pressure Side

In Figure 4.10 Pressure-Hub, the contour plots on the pressure side highlight a significant decrease in the heat transfer coefficient. This decrease can be attributed to the formation of a large wake on the pressure side caused by a high angle of attack. Both the SST transition model and the k-ω model reveal similar predictions for the heat transfer coefficient on the pressure side. This similarity arises from the fully turbulent nature of the flow due to extensive flow separation, leading to a consistent behaviour in the predictions of both models.

Figure 4.10(b) depicts the HTC over the polyline located on the pressure side at 25% span of the OGV. In both experimental and CFD results, an abrupt drop in HTC is observed. However, as we move towards the aft, there is a subsequent increase in HTC. This increase can be attributed to the interaction between the recirculating flow and the aft surface of the vane. This interaction promotes effective mixing, leading to an enhanced heat transfer coefficient towards the aft region. The 2D Off-design analyses added to the Appendix A.0.1 can be a good reference to observe the velocity contour for off-design analysis.

4.4.3 Hub

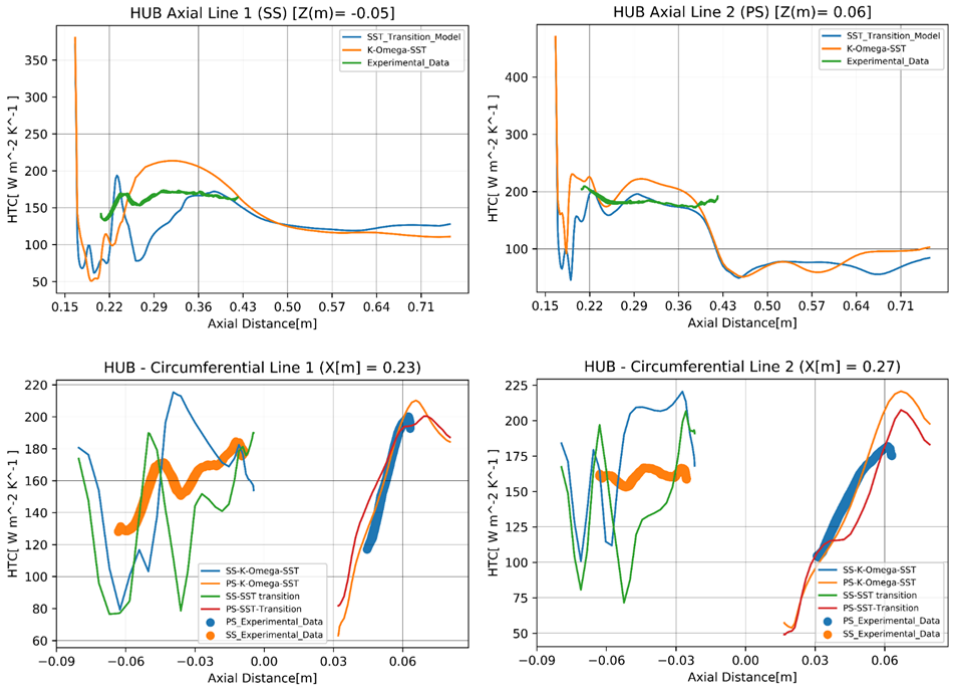

Figure 4.11: HTC HUB - Experimental vs CFD comparison over the defined polylines

By examining the HTC contour plots for the HUB in Figure 4.9, it is evident that a higher heat transfer is observed compared to the on-design analysis. This increase in heat transfer is because of the extreme angle of attack (AOA) of the incoming flow. Both the CFD models predict the same HTC profile, but the k-ω SST model exhibits higher heat transfer at the leading edge and around the suction side of the vane.
A more detailed observation can be interpreted from the figure 4.11. From the detailed analysis of figure 4.11, it's observed that the experimental results are in-between the HTC ranges predicted by SST Transition model and k-ω SST model, where the SST Transition model predicts a similar profile to the experimental data, but with a high fluctuation in predicted values.

4.4.4 Shroud

The shroud heat transfer results reveal a significant increase in HTC over the surface of the shroud, particularly around the leading edge of the vane and the suction side. Towards the pressure side of the OGV, the flow appears to be unstable, exhibiting transient effects associated with wake shedding. Both SST Transition model and k-ω SST model predict similar heat transfer results, although the k-ω Model shows a higher HTC over the suction side of OGV vane. In general, the predicted HTC for off-design analysis is way higher than the results obtained from on-design analysis.

The formation of strong horseshoe vortex at the leading edge of the vane is the reason for this increase in HTC around the OGV.

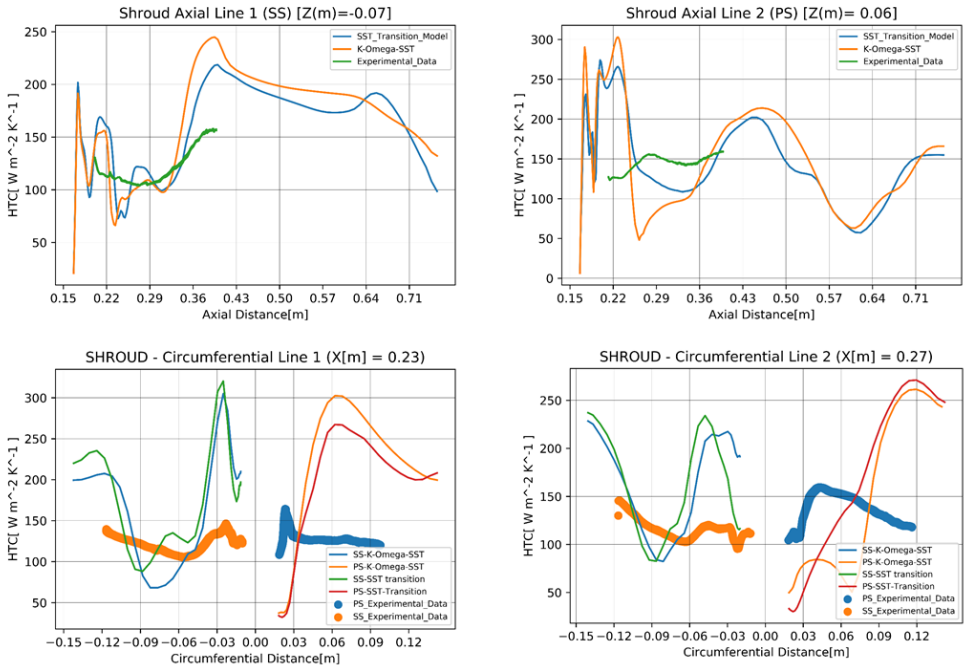

Figure 4.12: HTC SHROUD - Experimental vs CFD comparison over the defined polylines

The polyline data over the shroud shown in figure 4.13 gives a similar inference as seen for hub surface. The SST transition predicts the same HTC profile as experimental data, but with high fluctuation in the value.

4.5 Off-design Transient Analysis

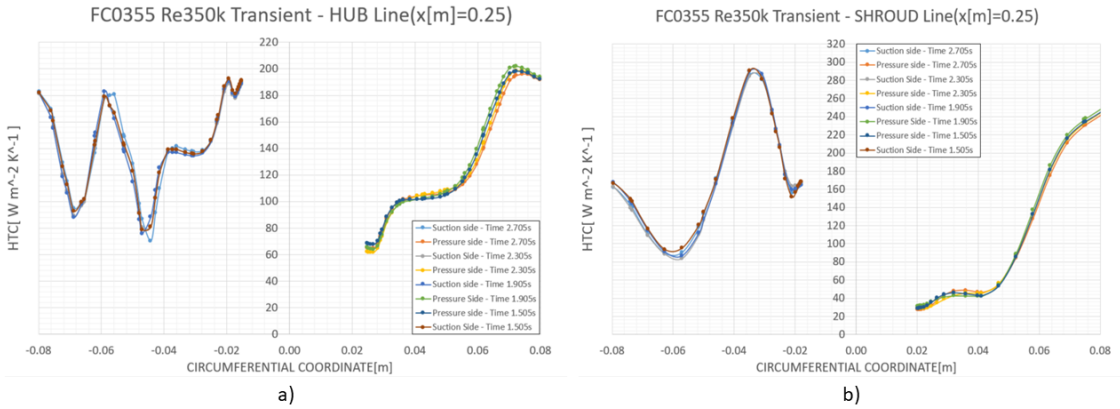

Figure 4.13: **(a)** HTC - Polyline over Hub Surface | **(b)** HTC - Polyline over Shroud Surface

Considering the earlier observations, it becomes evident that the off-design displays a transient nature, depicted by wake shedding occurring on the pressure side of the OGV due to high-angle-of-attack flow. To explore these transient influences on heat transfer, a transient analysis of the off-design scenarios has been conducted. The flow Courant number is adjusted to a maximum value of 0.7, with a time increment (ΔT) of 2e-5 seconds. The analysis runs for a total of 1,360,000 time steps, equivalent to a duration of 2.705 seconds of analysis. For detailed conclusions, a measurement polyline is defined at an axial distance of 0.25 meters from the reference point. The HTC results over specific time intervals 1.505s, 1.905s, 2.305s, and 2.705s are presented in Figure 4.12 for both the hub and shroud surfaces.

Upon evaluating the results depicted in Figure 4.12, it is evident that the transient flow characteristics have minimal influence on the end walls and vane heat transfer. The HTC over both the hub and shroud surfaces demonstrate negligible differences in the predicted heat transfer for all the examined time intervals.

4.6 Purge Inflow - 2D analysis

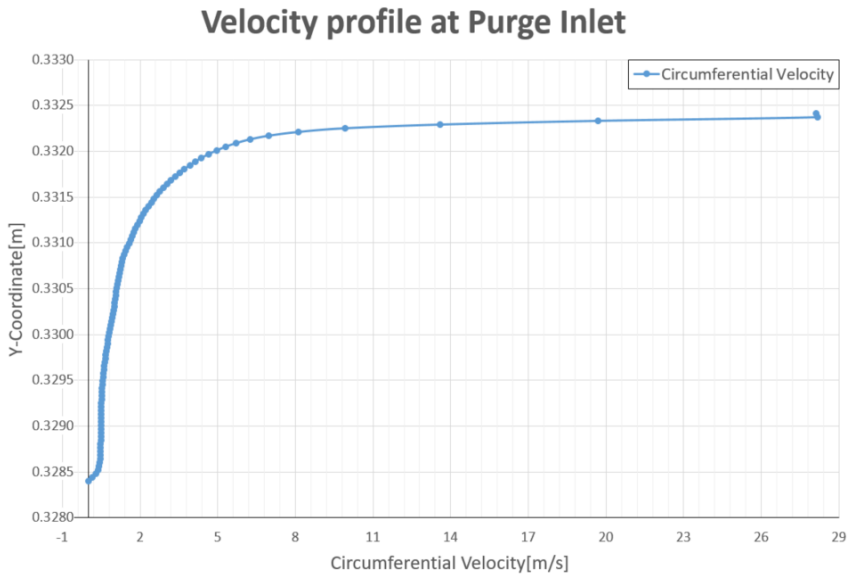

Figure 4.14: Circumferential Velocity over the purge inlet

The geometry defined in section 3.1.1.3 is utilized for purge-inflow analysis. The aim of this section is to evaluate the swirl component of flow exiting the purge inlet. The circumferential velocity at the purge inlet is given in figure 4.14. From the plot, it is observed that for the majority of the purge inlet, the circumferential velocity is below 2[m/s]. Only towards the rotor wall, the purge flow is affected by the rotation of the turbine rotor. The average velocity at purge inlet is measured to be 2.40929 [m/s]. This analysis serves as an inlet boundary condition for 3D purge analysis.

4.7 Purge 3D analysis

As mentioned in Section 3.5, a purge flow analysis is conducted to assess the film coefficient formed over the hub surface. The modified 1.5 stage model, as discussed in Section 3.1.2.2, is employed to extract the boundary conditions at the inlet and exit planes of the TRS domain. The only TRS domain is utilized to perform simulation using the SST Transition model. Furthermore, the impact of the turbulence model on film coefficient prediction and the influence of the swirl component at the purge inlet on the formed film is also evaluated. A comprehensive discussion is provided for each of these segments in the subsequent sections.

In all the purge flow analyses conducted, the geometrical walls are assumed to be adiabatic in order to evaluate the film coefficient. The formed film coefficient is measured by setting the temperature difference between the main flow and the purge flow to ΔT=10 K. Figure 4.15 illustrates the measured film coefficient for the on-design analysis, along with the experimental data. Figure 4.17 illustrates the measured film coefficient for the off-design analysis, along with the experimental data.

4.7.1 On-Design

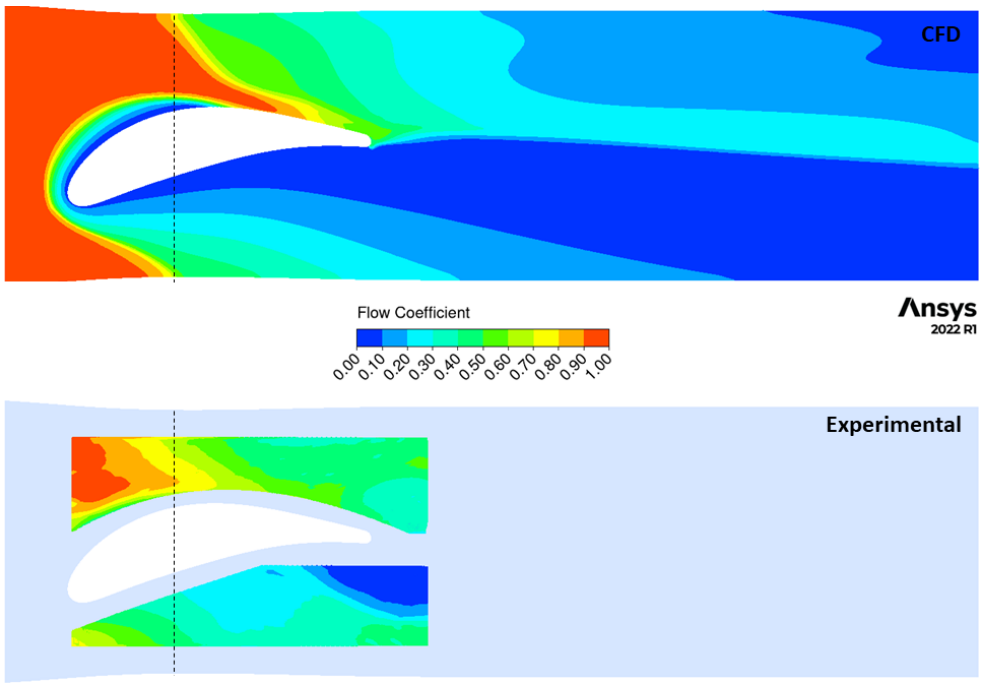

Figure 4.15: A HTC comparison between experimental results and CFD results for On-design case

The film coefficient provides information about the distribution of the purge flow film over the hub surface. A higher film coefficient indicates that the cold film has maximum intensity in that particular region, whereas a lower film coefficient suggests a weaker film presence. In the case of the on-design analysis, it is observed

that the cold film breaks down around 60% of the chord length. On the suction side, the film tends to move towards the surface of the OGV and eventually breaks down. This cold flow affects a significant portion of the suction side of the vane. Towards the aft of the hub, there is a noticeable breakup of the film. The profile predicted by the CFD simulation shows similarity to the experimental profile, although the experimental profile exhibits greater dispersion in comparison.

For a detailed comparison, a line is defined at an axial distance of 0.25[m] and the film coefficient over this line is obtained and compared against experimental data in figure 4.16. Notably, the experimental and CFD results exhibit reasonable alignment in the predicted profile.

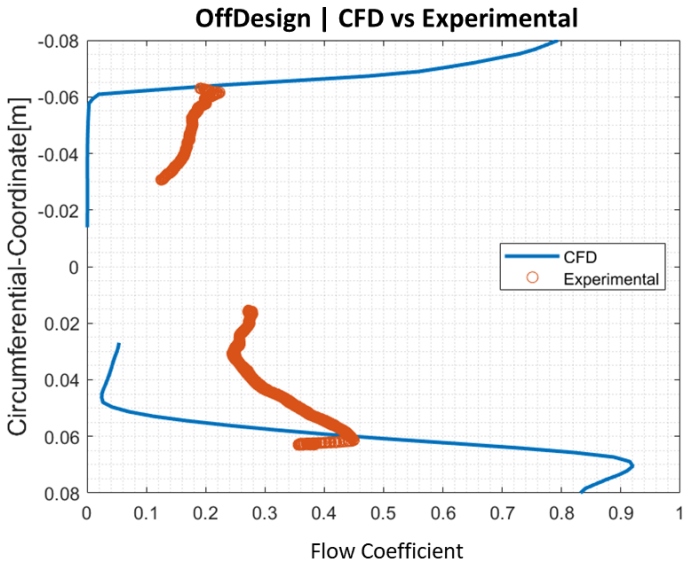

Figure 4.16: HTC comparison over the defined polyline between CFD and experimental results for on-design case

4.7.2 Off-design Analysis

The film coefficient contour from off-design purge is shown in figure 4.17. The figure 4.18 the observed HTC over the defined polylines. When examining the HTC contour plots, it becomes evident that film breakup occurs earlier in the off-design analysis due to the higher angle of attack of the incoming main flow. The cold film breaks up even before reaching the surface of the OGV. In the case of the off-design analysis, the cooling of the hub with the purge flow is less effective. This is primarily attributed to the high re-circulation occurring on the pressure side, which tends to draw the majority of the cold film towards that region.

Analyzing the HTC results observed at the defined polyline, both the experimental and CFD data exhibit a similar profile, but there is a significant variation in the predicted magnitude of the film coefficient. The experimental results demonstrate higher dispersivity, while the CFD results display a sudden breakup of the cold film.

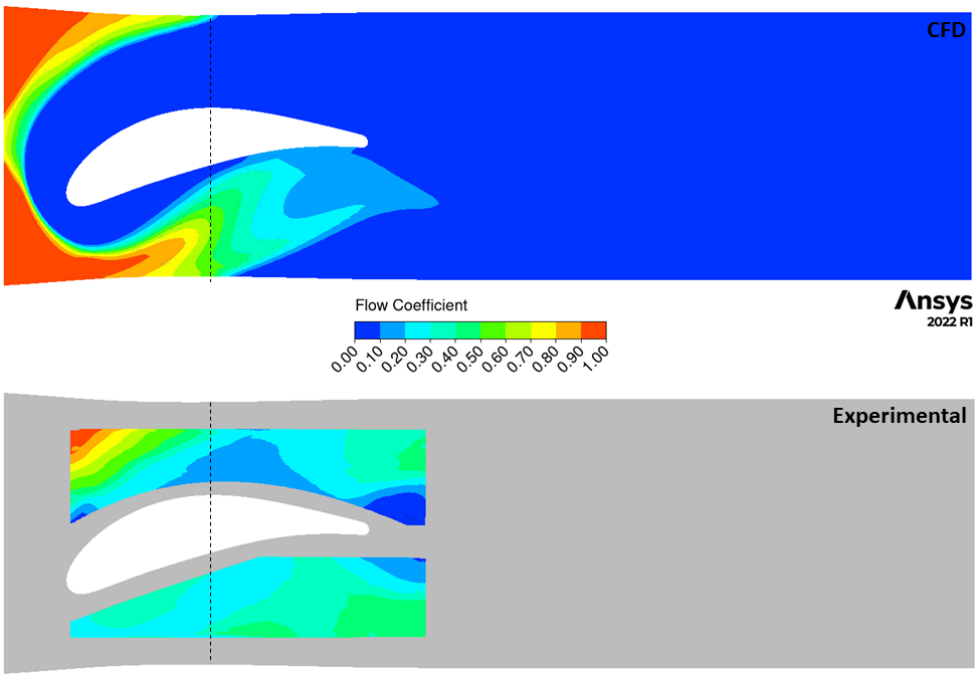

Figure 4.17: A HTC comparison between experimental results and CFD results for Off-design case

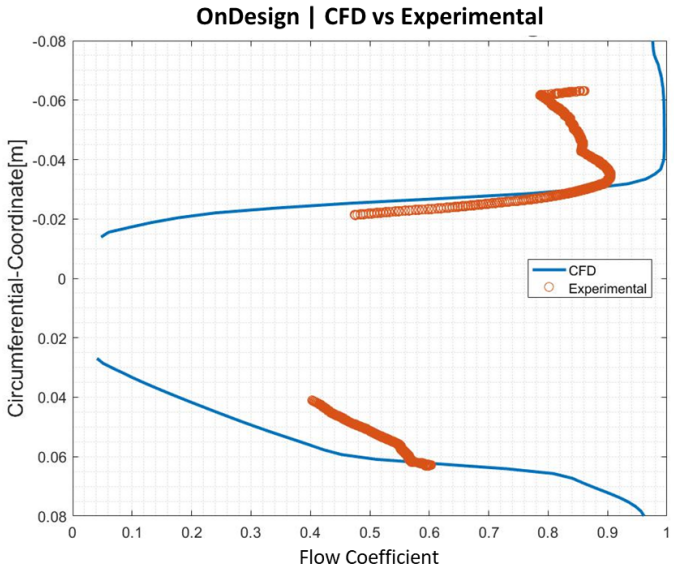

Figure 4.18: HTC comparison over the defined polyline between CFD and experimental results for off-design case

It is important to note that due to the limited availability of experimental data around the OGV, it is challenging to arrive at a definitive conclusion regarding the film behavior in that specific region.

4.7.3 Effect of Turbulence model

To assess the impact of turbulence models on predicting the film coefficient, the analysis was conducted using two turbulence models, namely k-ω SST and SST Transition, for the on-design analysis. The film coefficient contours resulting from these two analyses are depicted in Figure 4.19.

Upon examination, it is observed that the film coefficient profiles predicted by both turbulence models exhibit a similar overall shape with minor variations. The only noticeable difference occurs towards the suction side where the cold film interacts with the OGV surface. Overall, both turbulence models provide similar predictions of the film coefficient.

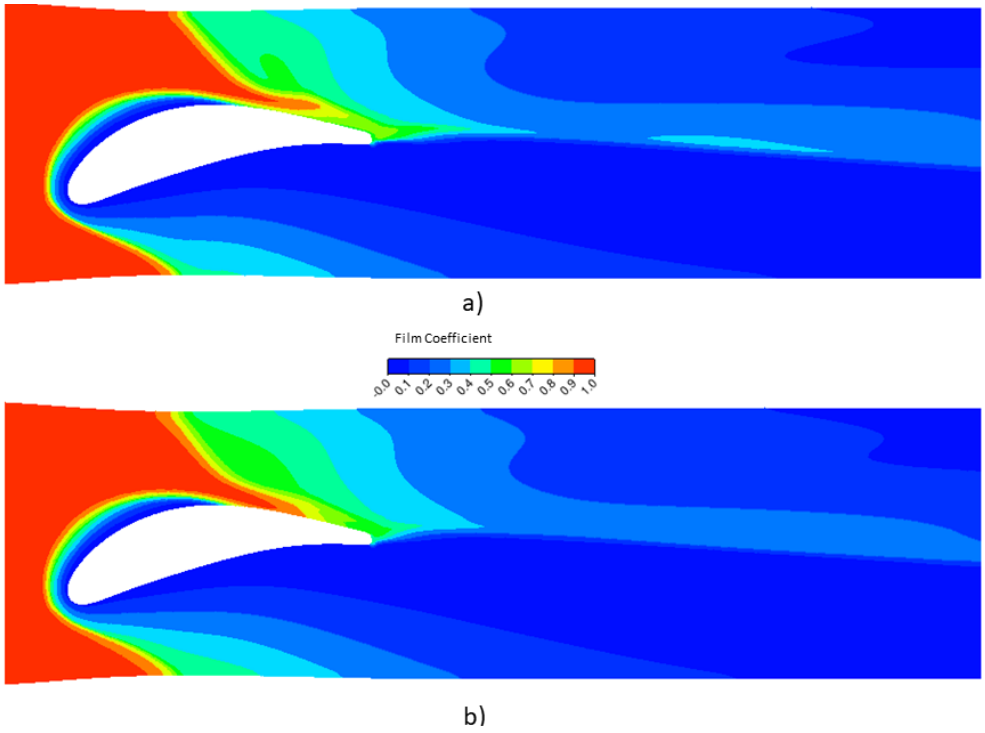

Figure 4.19: **(a)** Film Coefficient - k-ω SST model **(b)**Film Coefficient - SST Transition Model

4.7.4 Effect of pruge inlet swirl

As outlined in Section 4.6, an analysis was conducted to determine the swirl component at the purge inlet. The analysis revealed that the majority of the inlet flow exhibited no swirl, with the inlet region closer to the rotor domain exhibiting the highest velocity, as depicted in Figure 4.14.

All previous analyses on the purge flow were evaluated using only the axial component for the purge flow. To assess the effect of the circumferential velocity on the purge flow, a comparison was made between an analysis with 10%(of Rotor Velocity) circumferential component and an analysis without circumferential component. The 10% swirl component corresponds to a circumferential velocity of 2.8 m/s.

The film coefficient contours for these two cases are presented in Figure 4.20. From the results, it can be observed that the swirl component has minimal effect on the formed film coefficient. Both cases exhibit similar results, with only minor variations observed near the suction side where the flow attaches to the surface of the OGV.

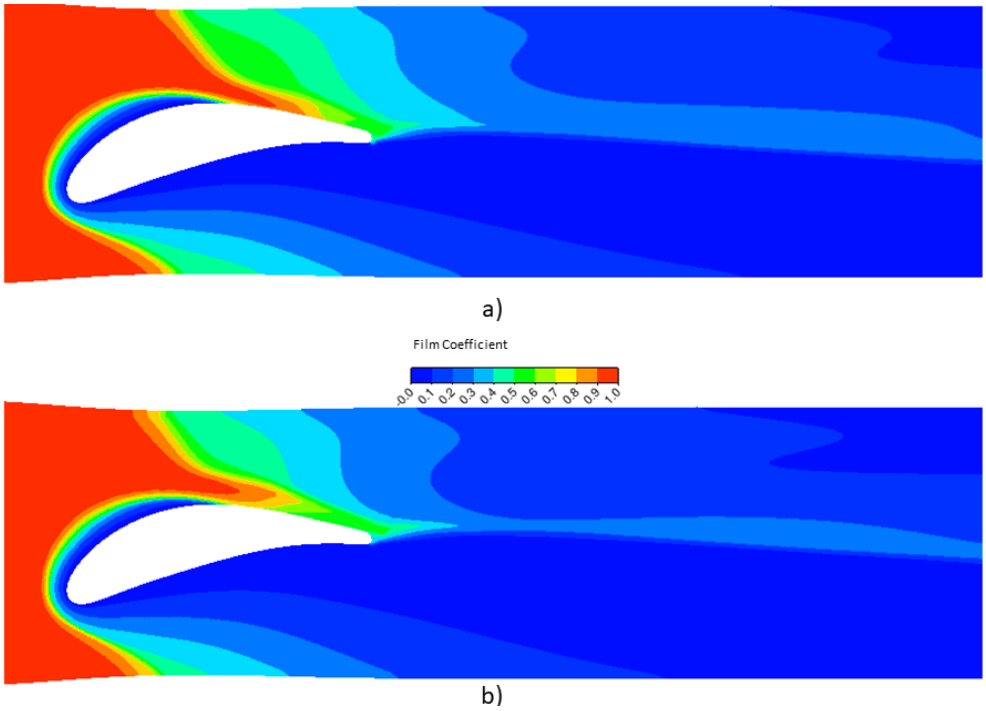

Figure 4.20: **(a)** Film Coefficient - No swirl component **(b)**Film Coefficient - 10% Swirl Component

4.7.5 Streamline-Visualization of purge flow

To visualize the breakup of the cold film in three dimensions, a turbo line is defined at the inlet surface near the hub region, specifically at a circumferential coordinate of 0.01 m. This turbo line is used for visualization purposes, and streamlines are released to analyze the pathway of the purge flow and examine the detailed breakup of the cold film.

Figure 4.21 depicts the streamlines over the suction and pressure sides for both the on-design and off-design analyses. figures (a) and (c) correspond to the off-design analysis, while figures (b) and (d) correspond to the on-design analysis. Upon examining the streamlined contours, several observations can be made. In the on-design

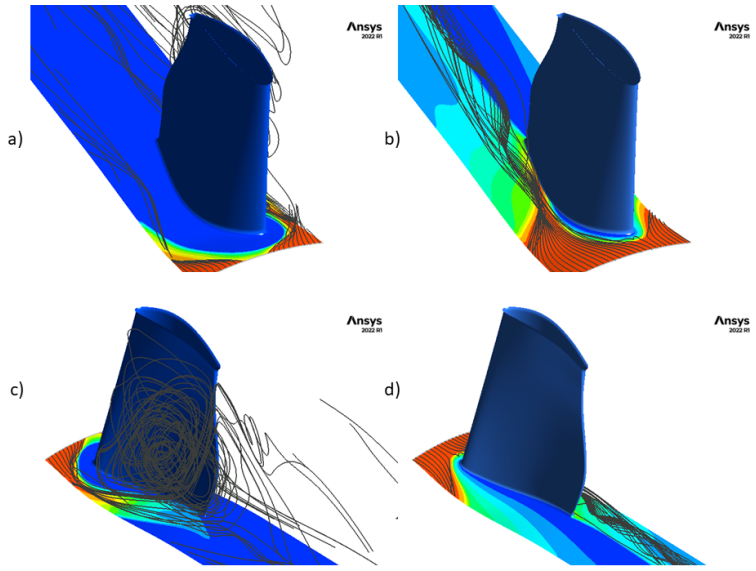

Figure 4.21: Streamline from the inlet of TRS domain near hub region

analysis, the flow is influenced by the formation of a horseshoe vortex at the leading edge of the OGV. In contrast, for the off-design analysis, a significant portion of the flow gets mixed with the recirculating flow occurring over the pressure side. The presence of a highly recirculating flow on the pressure side leads to an immediate breakup of the cold film.

5

Conclusion

The heat transfer analysis of the outlet guide vane has revealed several key findings. Firstly, it's observed that the flow transition happens over the suction side of the vane. Furthermore, the end wall flows have been identified as fully turbulent. The SST Transition model demonstrates remarkable capability in predicting heat transfer for flows with transition. However, the SST Transition model shows some limitations. It under-predicts the heat transfer when compared with experimental measurements. The primary reason for this discrepancy is attributed to the unsteady effects present in the upstream turbine domain, which are not fully accounted for in the model. Additionally, the k-ϵ model used in the analysis exhibits poor predictions, especially in its inability to accurately predict the boundary layer with an adverse pressure gradient.

In the off-design analysis, which investigates the OGV heat transfer under non-optimal operating conditions, a higher heat transfer has been observed in comparison to the on-design analysis. The CFD predictions for heat transfer on the end walls exhibit higher variations. The transient analysis conducted under off-design conditions demonstrates that the predicted heat transfer remains relatively unaffected by transient fluctuations or wake shedding. However, for the off-design analysis, the experimental results indicate that the purge cold film breaks down immediately upon entering the TRS HUB. On the other hand, for the on-design analysis, the purge cold film breaks down at approximately 60% of the vane chord, suggesting that it has a more significant impact on vane suction side heat transfer. Furthermore, when considering purge flow, the experimental results reveal a higher dispersivity compared to CFD predictions.

5.0.1 Recommendation for Future Work

1. The limited availability of experimental data around the OGV fillet and front side of TRS Hub, conducting additional experiments or obtaining more data in these specific regions would greatly benefit the analysis. This data would provide a more comprehensive understanding of the flow and heat transfer characteristics, leading to more accurate predictions and insights.
2. Perform a transient 1.5 stage analysis with sliding mesh capability to investigate the effect of upstream turbulence on the predicted HTC. This dynamic analysis will help capture the temporal variations in flow patterns and turbulence, improving the accuracy of heat transfer predictions under varying operating conditions.

3. Conduct an in-depth study of the behavior of the mixing plane in the 1.5 stage analysis. Understanding the mixing plane's performance and its influence on the overall flow field can lead to more realistic simulations, allowing for better comparison with experimental data and more reliable conclusions.
4. Include the rim cavity as a 3D domain in the 1.5 stage model. This enhancement will enable a more detailed representation of the flow and heat transfer phenomena occurring within the rim cavity, providing valuable insights into its interactions with adjacent turbine components and improving the overall accuracy of the analysis

Bibliography

[1] I. Jonsson, V. Chernoray, and R. Dhanasegaran, "Infrared thermography investigation of heat transfer on outlet guide vanes in an engine exit module," 2019.

[2] L. Wang, B. Sunden, V. Chernoray, and H. Abrahamsson, "Endwall heat transfer measurements of an outlet guide vane at on and off design conditions," 2013.

[3] L. Wang, B. Sundén, V. Chernoray, and H. Abrahamsson, "Experimental Study of Endwall Heat Transfer in a Linear Cascade," in *Journal of Physics Conference Series*, ser. Journal of Physics Conference Series, vol. 395, Nov. 2012, p. 012028.

[4] C. Wang, L. Luo, L. Wang, B. Sundén, V. Chernoray, C. Arroyo, and H. Abrahamsson, "Experimental and numerical investigation of outlet guide vane and endwall heat transfer with various inlet flow angles," *International Journal of Heat and Mass Transfer*, 2016. [Online]. Available: https://www.sciencedirect.com/science/article/pii/S0017931015302118

[5] C. Wang, L. Wang, B. Sunden, V. Chernoray, and H. Abrahamsson, "An experimental study of heat transfer on an outlet guide vane," *Proceedings of the ASME Turbo Expo*, vol. 5, 2014.

[6] S. Deshpande, I. Jonsson, and V. Chernoray, "Effect of surface roughness on aerodynamic performance of turbine rear structure," 2019.

[7] A. H. Mattia Nillson, Srikanth Deshpande, "Aero-validation of cfd methods for turbine rear structures using experimental data"," vol. 1, 2020.

[8] M. S. B. Frank Kreith, Raj M. Manglik, "Principles of heat transfer," vol. Sixth Edition.

[9] L. Davidson, "Fluid mechanics, turbulent flow and turbulence modeling," 2022.

[10] Fluid mechanics 101 learn the fundamentals of computational fluid dynamics. [Online]. Available: https://www.fluidmechanics101.com/

A

Appendix 1

A.0.1 2D OGV Vane

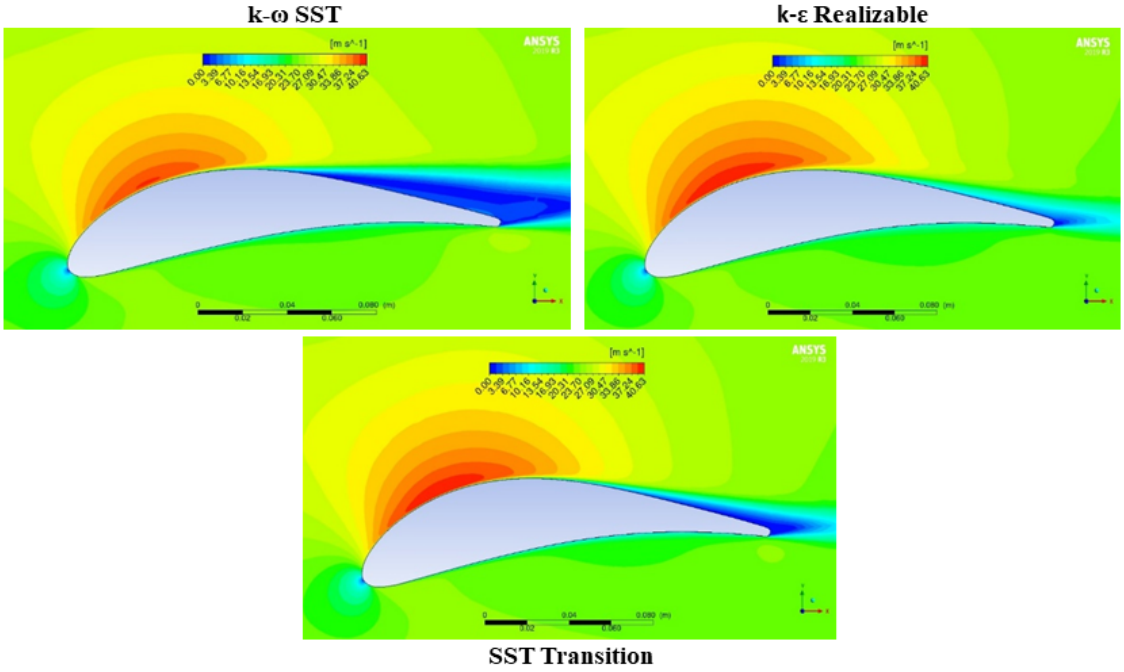

Figure A.1: 2D analysis - On design - Velocity Magnitude

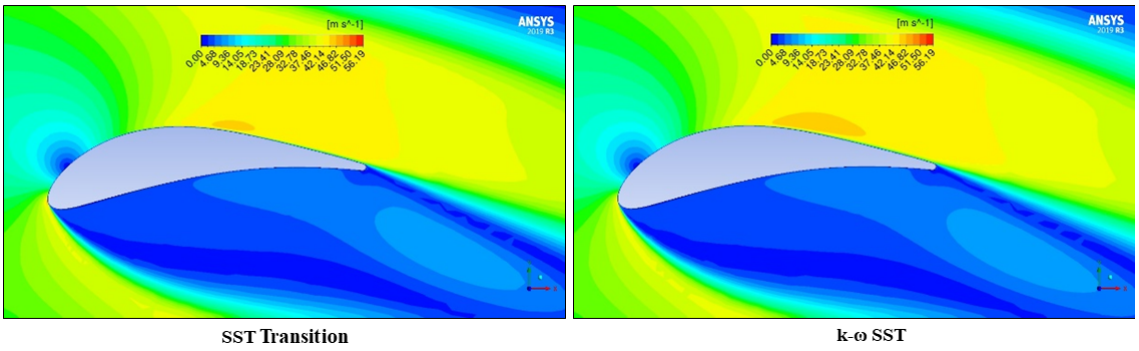

Figure A.2: 2D analysis - Off design - Velocity Magnitude

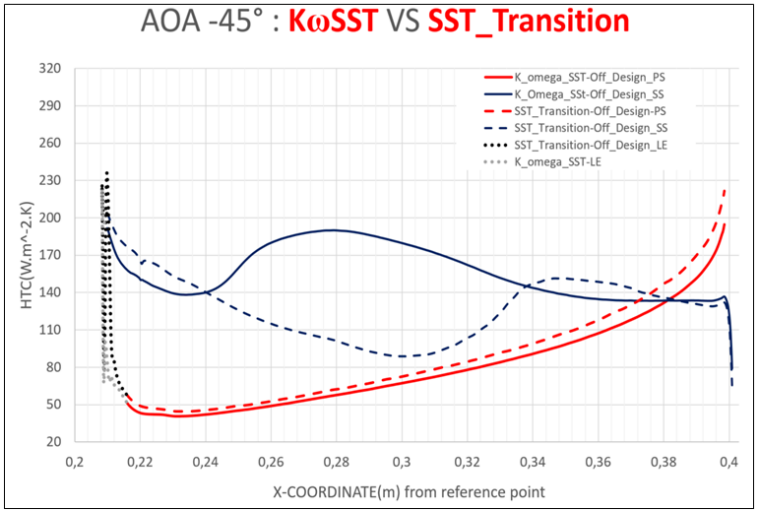

Figure A.3: HTC - comaprison for off design analysis simulated using k-ω SST and k-ϵ Realizable.

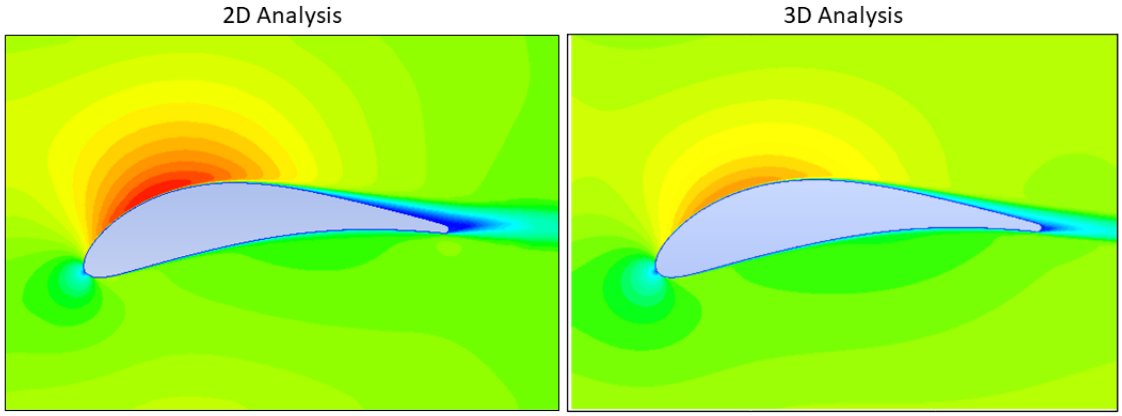

Figure A.4: 2D Vs 3D Analysis - Velocity Magnitude

A.0.2 Purge Inflow - 2D Analysis

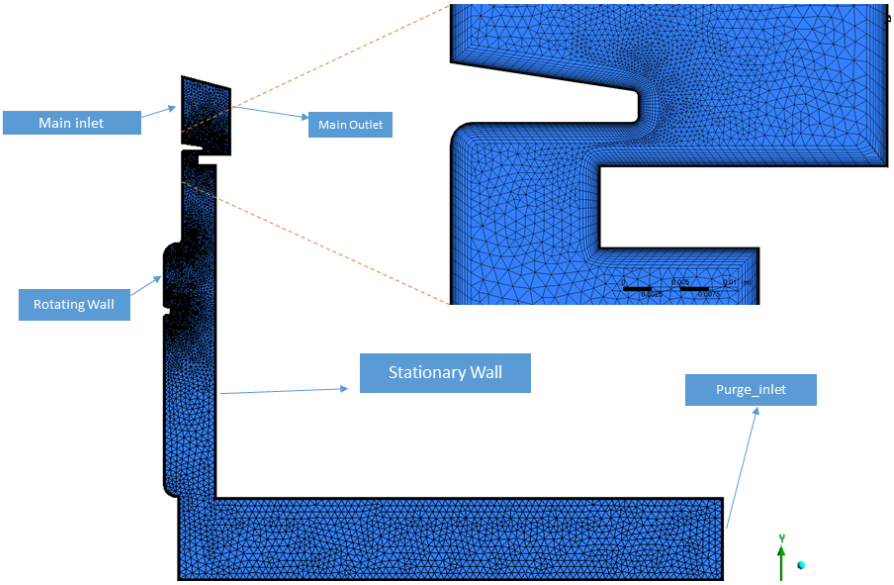

Figure A.5: Purge Inflow Domain - Mesh

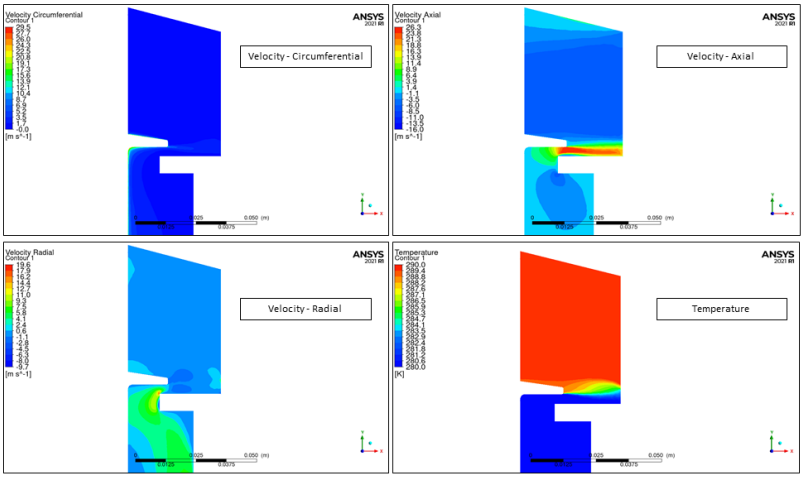

Figure A.6: Purge Inflow - Contour Plots

A.0.3 3D On design

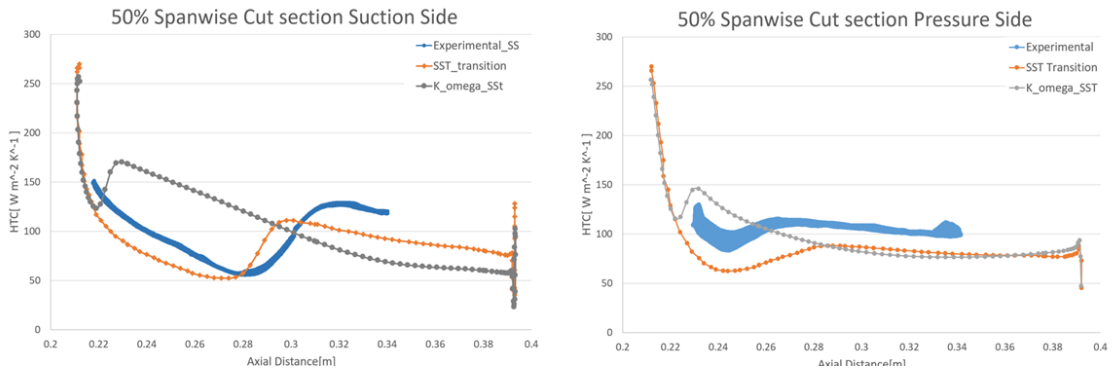

Figure A.7: HTC over 50% OGV Spanwise cut section - On Design

A.0.4 3D Off design

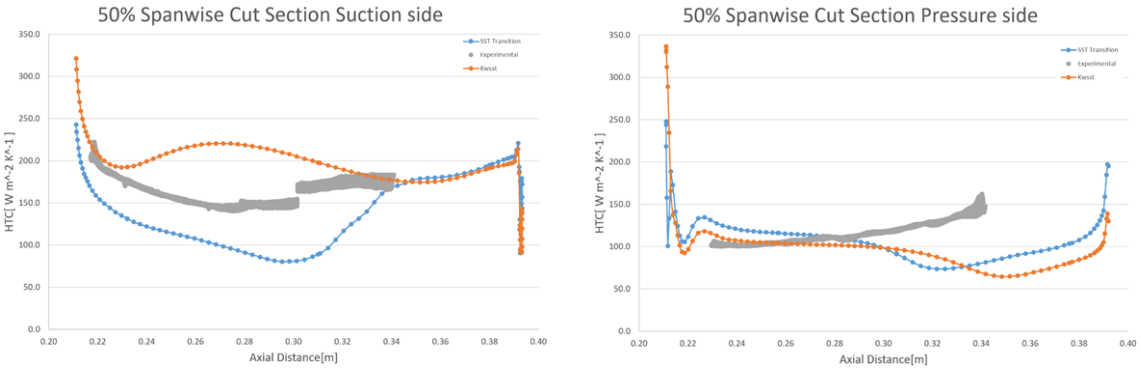

Figure A.8: HTC over 50% OGV Spanwise cut section - Off Design

A.0.5 3D offdesign Transient analysis

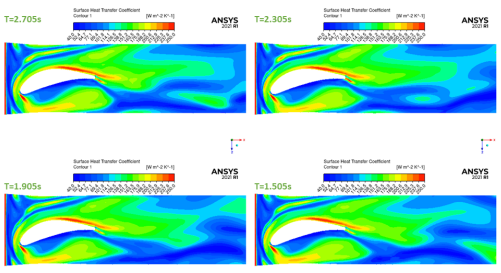

Figure A.9: HUB - HTC Contour from transient analysis

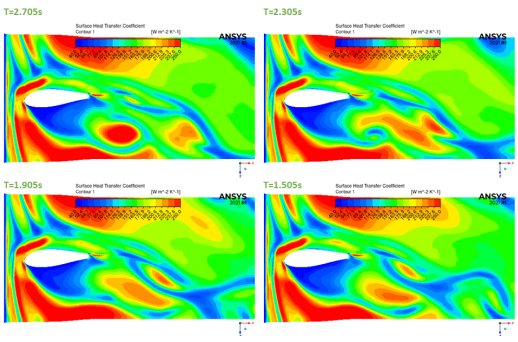

Figure A.10: SHROUD - HTC Contour from transient analysis

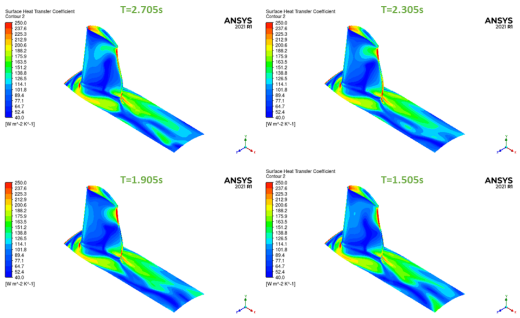

Figure A.11: Pressure side of OGV - HTC Contour from transient analysis

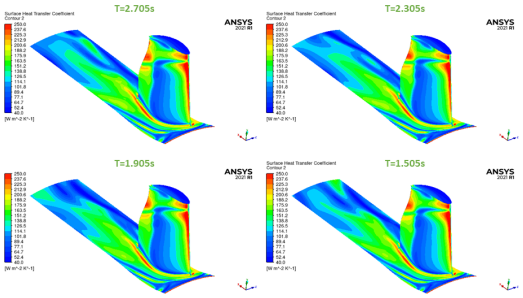

Figure A.12: Suction side of OGV - HTC Contour from transient analysis

.

DEPARTMENT OF SOME SUBJECT OR TECHNOLOGY
CHALMERS UNIVERSITY OF TECHNOLOGY
Gothenburg, Sweden
www.chalmers.se

CHALMERS
UNIVERSITY OF TECHNOLOGY